Title
Molecular drivers of the macronuclear shape change cycle in Stentor coeruleus

Author
McGillivary, Rebecca Marianne

Publication Date
2021

Peer reviewed|Thesis/dissertation

Molecular drivers of the macronuclear shape change cycle in Stentor coeruleus

by
Rebecca McGillivary

DISSERTATION
Submitted in partial satisfaction of the requirements for degree of
DOCTOR OF PHILOSOPHY

in

Cell Biology

in the

GRADUATE DIVISION
of the
UNIVERSITY OF CALIFORNIA, SAN FRANCISCO

Approved:

DocuSigned by:
Dyche Mullins
E4FB70A20A7546F...

Dyche Mullins

Chair

DocuSigned by:
Wallace Marshall
5CCD5F2E84D9...

Wallace Marshall

DocuSigned by:
Barbara Panning
7BD74D2E31C74B7...

Barbara Panning

Committee Members

Acknowledgments

I am incredibly grateful to have had an abundance of support from colleagues, friends, and family during my Ph.D. journey.

A huge thank you to my advisor, Dr. Wallace Marshall, for his unwavering support in all things scientific, professional, and personal. This project had many moments when the data was more confusing than clarifying, but working with you always re-energized my love for science, and made graduate school an amazingly fun adventure.

Thank you to my committee members, Dr. Barbara Panning and Dr. Dyche Mullins. Your support from my time as a first year in classes, to my qualifying exam, and then during my thesis work helped shape me as a scientist.

I am grateful to my mentors from my undergraduate years at UCLA. Thank you to Dr. Ira Clark and Dr. Rafael Romero for being the first people to encourage me to pursue graduate studies. I also thank Dr. Margot Quinlan and Dr. Zeynep Durer for mentoring me during my undergraduate research, and for preparing me well for graduate school.

Thank you to my labmates, who were a joy to work with and who taught me so much. I am especially grateful to Dr. Mark Slabodnick, Dr. Pranidhi Sood, Dr. Sarah Reiff, Dr. Tatyana Makushok, and Dr. Athena Lin for all of their help and for teaching me how to work with *Stentor coeruleus.* I also thank Dr. Pranidhi Sood for contributing her RNA seq data on CSE1 in Chapter 2 - this was the foothold that allowed me to work on this project.

Thank you to Dr. Kasia Hammar for working with me on the transmission electron

microscopy experiments that are in Chapters 2 and 3. It was incredibly fun to learn about this technique from the expert.

I am grateful to have shared this graduate school experience with my classmates. Having this group of amazing people and scientists to share experiences with made the highs of graduate school even better, and the lows not as bad anymore. Extra thanks to Eliza, Mitch, Luke, Madeline, Rosa, and Paola - it was so much fun to go on adventures with you all in San Francisco and beyond.

Thank you to my family, for all of your love and support. To my brothers, Andrew and Alex, thank you for being there for me throughout college and graduate school - we are definitely a UC family! To my parents, Barb and Jim, thank you for everything. I could not have done any of this without your help; your support of my many interests throughout my life means the world to me.

To my husband, Daniel, I am so grateful to have had you by my side during this entire journey. I love you, and I am so lucky to have your support and friendship.

Contributions

Chapter 2 contains work from a preprint in bioRxiv:

McGillivary, Rebecca M., Pranidhi Sood, Katherine Hammar, and Wallace F. Marshall. 2021. "The Nuclear Transport Factor CSE1 Drives Macronuclear Volume Increase and Macronuclear Node Condensation in Stentor Coeruleus." bioRxiv. https://doi.org/10.1101/2021.09.21.461284.

Abstract

Molecular drivers of the macronuclear shape change cycle in *Stentor coeruleus*

by

Rebecca McGillivary

How nuclei are shaped within cells is one of the fundamental questions of cellular spatial patterning. This question has been mainly investigated in metazoan cells, as misshapen nuclei are prominent features of cancer and aging in humans. The giant ciliate *Stentor coeruleus* provides an opportunity to learn more about the mechanisms behind nuclear shape, because *Stentor* undergoes a dramatic and developmentally regulated nuclear shape change. During cell division and regeneration, the macronucleus dramatically changes shape before dividing amitotically into two daughter cells. The moniliform macronucleus condenses into single sphere, extends, and renodulates in 2-3 hours near the end of cell division and regeneration. It is unclear how this extreme macronuclear shape change is regulated. While microsurgical and electron microscopy studies addressed this question in the past, we have had virtually no molecular insight into this feat of subcellular morphogenesis. Here we identify the first molecular driver of macronuclear condensation: the nuclear transport factor CSE1. In

other model systems, CSE1 is needed to export importin-alpha, thus CSE1 is necessary for the overall import of proteins into the nucleus. In *Stentor*, we found that knocking down CSE1 using RNAi reduced the ability of *Stentor* to increase its macronuclear volume during condensation, and it also prevented the nodes from fusing together into a single mass. Immunofluorescence data showed that CSE1 is mainly cytoplasmic during interphase, and then becomes mainly intranuclear while the macronucleus is condensed. We also found that as the macronucleus elongates, its volume decreases, and there are no longer any detectable levels of CSE1 in the cell. This data comes together in our model of how CSE1 drives macronuclear condensation in *Stentor.* Increased nuclear import driven by CSE1 increases the volume of the macronucleus, and the macronucleus changes shape into a sphere to accommodate this volume increase. As CSE1 is degraded, nuclear export dominates, and the volume of the nucleus decreases, readying the macronucleus for elongation. In regards to the elongation and nodulation phases of the macronuclear shape change cycle, we report observations that may be useful for future investigations into these processes. We observed transient microtubule structures in and around the elongating macronucleus. These repeat observations that were made over 40 years ago. We also report a subtle nuclear node defect in *Stentor* that have a SUN homolog knocked down by RNAi, suggesting that the LINC complex may play a role in nodulation of the macronucleus. Overall, we report the first molecular players involved in the macronuclear shape change cycle, and help establish *Stentor coeruleus* as a model system for studying nuclear shape.

Contents

1 Introduction **1**

2 CSE1 drives macronuclear condensation **13**

2.1 Abstract 13

2.2 Introduction 14

2.3 Results 15

2.4 Discussion 28

2.5 Methods 35

2.6 Supplementary Figures 40

3 Macronuclear Elongation and Nodulation **53**

3.1 Introduction 53

3.2 Microtubules and macronuclear elongation 56

3.3 SUN proteins and macronuclear nodulation 60

3.4 Discussion 63

4 Dissertation Discussion **68**

4.1 CSE1's role in macronuclear condensation 69

4.2 Future directions for the study of elongation and nodulation 70

References **72**

List of Figures

1.1 Illustration of nuclear shapes found in mammalian cells 3

2.1 *Stentor* macronuclear structure 17

2.2 *Stentor* division and regeneration 18

2.3 Macronuclear volume change during regeneration 21

2.4 Expression of a CSE1 ortholog during macronuclear shape change 22

2.5 CSE1 homologs 24

2.6 Macronuclear cycle in CSE1 RNAi *Stentor* 25

2.7 Plots comparing CSE1 RNAi and non-RNAi macronuclear cycles 26

2.8 Effects of CSE1 RNAi over time 27

2.9 Dynamic relocalization of CSE1 during nuclear shape change 29

2.10 Model of CSE1's role in macronuclear condensation 30

2.11 Macronuclear volume calculation pipeline 41

2.12 Macronuclear volume during regeneration of non-RNAi *Stentor* 42

2.13 Macronuclear volume during regeneration of (*CSE1)RNAi Stentor* 43

2.14 Regeneration of *CSE1(RNAi) Stentor* 44

2.15 Peptide block of anti-CSE1 antibody 45

2.16 RNAi control for antibody specificity. 45

2.17 CSE1 localization CSE1 in methanol fixed *Stentor* during regeneration 46

2.18 Immunofluorescence of CSE1 in dividing *Stentor* fixed with methanol. 47

2.19 Alignment of both *Stentor* CSE1 genes 49

2.19 Multiple alignment of CSE1 genes 52

3.1 Transmission electron microscopy of elongating macronuclei 57

3.2 Immunofluorescence of microtubules during macronuclear elongation 59

3.3 RNAi of SUN homologs in *Stentor* 61

3.4 Length/width of nuclear nodes in *(SUN RNAi) Stentor* 62

List of Tables

2.1 List of RNAi constructs and primers used in this study 48

Chapter 1

Introduction

How cells create their diverse arrays of shapes and forms is one of the fundamental questions of cell biology. Since form and function are intimately linked, proper regulation of the size and shape of organelles is a crucial task that all cells must carry out. Despite the importance of this question, studying how cells shape their organelles has presented challenges. Organelles are complex structures made of many components. The regulation of their formation and their dynamics is similarly complex, requiring an interplay between genetic regulation and physical mechanisms.

The cellular structure that is among the most studied in this context is the cell nucleus. As the container of the cell's most precious cargo, the genome, the size and shape of the nucleus is under tight regulation. Cell biologists have long observed that cells maintain a constant nuclear:cytoplasmic ratio, and most metazoan cells have a spheroid nucleus [11] **(Figure 1.1)**. The importance of the shape and size of the nucleus are most apparent in

situations where they are misregulated. One of the main features that has been used to diagnose cancer for over 100 years is the shape of the nucleus. In cancer cells the nuclear shape is typically disrupted, having folds and irregularly shaped borders instead of being rounded [29]. The size is also altered to be either significantly larger or smaller than normal in many cancer types [29] **(Figure 1.1)**. Aging cells also follow similar trends - older cells tend to have irregularly shaped nuclei [50] **(Figure 1.1)**. The disease progeria causes early aging, and the shape of the nuclei from these patients are extremely wrinkled. This shape defect is linked to defects in lamins, the structural proteins that form a network beneath the nuclear envelope [25]. Normal aging in humans also causes nuclei to become misshapen, and it has been shown that this can also be attributed to changes in the nuclear lamina as we age [50]. In the cases of both natural aging and cancer, there are also a multitude of other mis-regulated genes, making both the causes and consequences of misshapen nuclei difficult to parse.

Non-spherical nuclear shapes can also be found in some differentiated animal cell types. In humans the most well-known example is the neutrophil nucleus. The human neutrophil nucleus has 2-5 irregularly-shaped lobes that are connected by thin regions [43] **(Figure 1.1)**. Neutrophils migrate throughout the body to reach sites of infection - to reach these areas, neutrophils must be extremely deformable. It has been proposed that the lobed shape of the neutrophil nucleus makes it more deformable, enabling the neutrophil to more easily squeeze through tight spaces. While the neutrophil nucleus is deformable due to the composition of its nuclear envelope, there is limited evidence supporting that the lobes themselves are

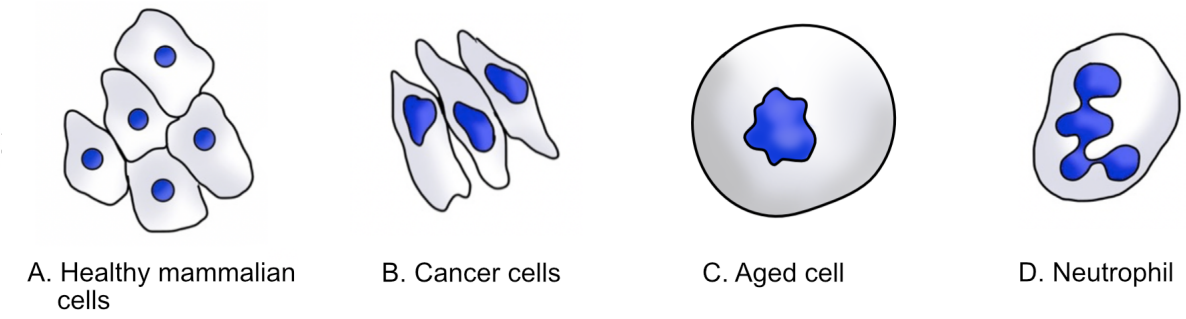

Figure 1.1: Illustration of nuclear shapes found in mammalian cells. A. Most healthy mammalian cells have spherical or spheroid nuclei. B. Cancer cells often exhibit large and wrinkled nuclei. C. Aged cells, through natural aging or in rapid aging diseases such as progeria, have wrinkled nuclear envelopes. D. Neutrophils have lobed nuclei that are highly deformable

necessary for this deformability [43]. Some hypo-lobulated neutrophils from patients with Pelger-Huët anomaly are able to migrate normally [43]. The role of the lobed nuclear shape in neutrophils is still an active area of investigation. Another place where non-spherical nuclei can be found is in the tadpole tail fin cells of *Xenopus tropicalis.* These cells possess extremely branched nuclei that are healthy and able to undergo mitosis [3]. To maintain this unusual nuclear shape, the nucleus needs to contain Lamin B1 and maintain contact with the actin cytoskeleton [3]. When the branched morphology of these nuclei is reduced, the development of the tail fin no longer proceeds normally - instead the tail fins developed with morphological defects that reduced the ability of the tadpoles to swim [3]. How the branched nuclear shape of these tail fin cells contribute to the overall structure of the tail fin is still an open question. Exactly how nuclear shape in metazoan cells affects cellular physiology has been difficult to ascertain even in cell types with non-spherical nuclei. What has emerged

is that the cytoskeleton and the nuclear lamina play important roles in modulating the deformability of the nucleus, allowing it to morph into shapes that are visually distinct from spheroid nuclei.

Nuclear shape has also been investigated by introducing mutations into cells that typically have spheroid nuclei. In *Saccharomyces cerevisiae*, mutations in the secretory pathway are sometimes associated with alterations in nuclear morphology - in particular, the *sec6-4* mutant strain develops a bilobed morphology because the growth of the nuclear envelope outpaces the growth of the nuclear volume [65]. It is thought that altering the shape allows the cell to accommodate the extra nuclear envelope without changing the volume of the nucleus. The state of chromatin in the nucleus has been shown to affect both the mechanical properties and the shape of the nucleus in mammalian cells, with euchromatin softening the nucleus and promoting blebs, and heterochromatin stiffening the nucleus [58]. A recent RNAi screen found a wide variety of chromatin modifying genes are necessary for maintaining a round nuclear shape [59]. Many of these genes are also commonly mutated in cancer, highlighting the strong link between nuclear shape and cancer [59].

Studying the regulation of nuclear shape is often difficult in metazoan cells because in most healthy cells the nuclei are consistently spheroid with very minor changes in size and shape. In the disease states that have misshapen nuclei, a wide variety of processes are misregulated. Despite these difficulties, studies in both cells that naturally have non-spherical nuclei, as well as studies that use mutations to alter the shape of rounded nuclei, have found general processes that cells use to shape their nuclei. The composition of the

nuclear lamina plays a major role in nuclear shape. As the main mechanical component of the nuclear envelope in metazoan cells, altering its composition can soften the nucleus, making it more deformable. The cytoskeleton also plays a role in nuclear shape as the main cytoplasmic component that applies force to the nucleus. This force is transduced to the nucleus through the linker of nucleoskeleton and cytoskeleton, the LINC complex - this force transduction has been most well studied in the context of nuclear positioning [6]. The LINC complex has also been found to facilitate the squeezing of nuclei through constricted spaces [7]. Chromatin has also been shown to affect the mechanical properties of the nucleus, with condensed heterochromatin generally stiffening nuclei [58] [57]. The dynamics of nuclear growth can also affect nuclear shape if the nuclear envelope and nuclear volume do not scale together such that they can remain a spherical shape [65]. The mechanisms that shape nuclei in animal and fungal cells are complex, and are also closely linked to other cellular processes. The effects of altered nuclear shapes on the physiology of the cell have also been difficult to study in many cases.

The study of how cells shape their nuclei can benefit from a model system with a nucleus that undergoes an obvious shape change that occurs as a part of a developmental process. The developmental process will help us identify genes that are candidates for nuclear shape regulation. A nucleus with a clear shape change will allow us to notice if altering a candidate gene is having an effect on nuclear shape. These two components together will allow us to more easily study the regulation of nuclear shape, with the hope that in the future we can then apply this knowledge to the study of metazoan cells.

Any model organism search that is looking for interesting nuclear biology must consider ciliates. This extremely diverse group of single-celled eukaryotes are all linked by two main features: complex microtubule cortexes covered in motile cilia, and the possession of two differentiated types of nuclei [42]. Ciliates have both an asexual and sexual lifecycle. The cells can vegetatively divide on their own to produce offspring, or they can mate with each other to intermix their genes [42]. The larger nucleus, aptly named the macronucleus, is a polyploid nucleus that carries out the transcriptional activity needed in the vegetative life of the ciliate. The smaller micronucleus acts as a germline nucleus, and is typically transcriptionally silent [42]. The behavior of the macro- and micronuclei in both lifecycles varies among different species [42].

The two main groups of ciliates are each defined by how their macronuclei behave during vegetative cell division [23]. Intramacronucleata, which includes the most widely studied model ciliates like *Tetrahymena*, *Paramecium*, and *Oxytricha*, divide their macronuclei amitotically using both intranuclear and extranuclear microtubules [42]. The other group, heterotrichea, contains some of the largest ciliates like *Stentor*, *Blepharisma*, and *Spirostomum*. Heterotrichs are able to divide their macronucleus amitotically, but they only have extranuclear microtubules [42]. It is currently a matter of debate whether Heterotrichs lost their intranuclear microtubules, or if they independently evolved a strategy to divide their macronuclei. In either case, it is clear that the macronuclei of heterotrichs are evolutionarily and morphologically distinct from even the more well-known model ciliate species.

Heterotrich macronuclei are interesting candidates for studying nuclear shape, because

their shapes vary dramatically from species to species, and some have the ability to change shape during the lifecycle of the cell. Small species of *Stentor*, like *Stentor multiformis*, have spherical macronuclei. Intermediately sized *Stentor* species like *Stentor roseli*, have vermiform macronuclei. The large species of *Stentor*, like the 1 mm long *Stentor coeruleus*, have moniliform macronuclei that appear as a chain of nodes just beneath the cell cortex [63]. Other large heterotrichous ciliates such as the 4 mm long *Spirostomum ambiguum* also have moniliform macronuclei [45]. The moniliform macronuclei of these species also dramatically change shape as a normal part of their cell cycles. The nodes of the moniliform macronuclei condense into a single sphere, elongate into a vermiform shape, and then re-nodulate back into their original moniliform shape [63]. This process happens during cell division, though the exact timing of these events relative to the other processes of cell division varies depending on the species. In *Spirostomum* for example, the moniliform macronucleus condenses, then takes 5 hours to elongate into a vermiform shape. Four hours after this stage, cytokinesis is completed and the vermiform macronucleus is cleaved in two. The macronucleus nodulates 24-48 hours after cell division as the half-length daughter cells grow to their full length [45].

Stentor coeruleus stands out as an excellent organism to study this type of dramatic macronuclear shape change, because it carries out these morphological stages much more quickly. While *Spriostomum's* macronuclear shape change cycle takes place over a span of roughly 2 days, *Stentor's* completes its macronuclear shape change cycle in only 2 hours. *Stentor's* macronucleus also carries out this same shape change during regeneration in addition to cell division [63]. *Stentor* are cone-shaped cilates, with a large ciliated oral apparatus

at the wider anterior end. Removing this oral apparatus by either cutting or by sucrose shock initiates the regeneration process [61] [63]. This regeneration process has many similarities to cell division. A new oral apparatus is formed on the side of the cell and moves to the anterior just as it does when the cell is preparing to divide. The macronucleus also undergoes the same shape change cycle that it undergoes during cell division [63]. The only morphological difference is that cytokinesis and the splitting of the macronucleus does not take place during regeneration [68]. In *Stentor* it is easy to induce a rapid, dramatic, and developmentally regulated nuclear shape change in many cells simultaneously, making it a powerful model system in which to study nuclear shape change.

Previous researchers have taken note of the advantages of studying *Stentor's* macronucleus, and there is a fair amount of classical literature investigating the structure, positioning, size, and shape change of the macronucleus. *Stentor's* wound healing ability and large size made it amenable to microsurgical and grafting experiments. The macronucleus can be entirely removed - these studies showed that enucleates are able to swim and feed, but cannot digest food, and eventually die [63]. Enucleating stentors early in oral regeneration halts the process - but once the oral apparatus is constructed, enucleating the stentor does not prevent its migration to the anterior of the cell [63]. A single node of the macronucleus, however, is enough for regeneration to take place normally [60]. There is no clear evidence that there is any difference between the nodes' abilities to facilitate regeneration, however there is a study that suggests the most posterior node is sometimes unable to support regeneration [67]. Overall, most studies suggest that each node of this highly polyploid macronucleus

has at least one complete copy of the genome, and can therefore support the regeneration of all cellular structures. The nucleus:cytoplasm ratio of *Stentor* can also be dramatically altered using grafting techniques. Hyper-nucleated stentors gradually reduce their nuclear volume to their normal ratio, while hypo-nucleated stentors tend to have delayed starts to regeneration [62].

Grafting experiments have also been used to investigate the macronuclear cycle itself. The macronucleus does not autonomously go through its shape changes - instead it is dependent on the state of the cytoplasm at different stages. Three hours after sucrose shock is a critical time for macronuclear condensation - macronuclei transplanted before this time are able to condense, while macronuclei that are transplanted after this timepoint are generally unable to condense [18]. The condensed macronucleus also relies on cytoplasmic factors for elongation to take place. A condensed macronucleus transplanted into a non regenerating cell will fail to elongate and have incomplete node formation [18].

Electron microscopy experiments have also investigated the structural changes that the macronucleus undergoes during the macronuclear shape change cycle. In non-regenerating cells, heterochromatin and euchromatin are dispersed throughout the nucleoplasm - there is no peripheral heterochromatin like one might observe in metazoan cells [47]. When the macronucleus is condensed, the chromatin appears to be completely homogenous [47]. This is also the time at which DNA replication, normally an ongoing process in the *Stentor* macronucleus, is halted [17]. During macronuclear elongation, microtubules surrounding the macronucleus are visible with electron microscopy [47] [46]. This is similar to electron

microscopy images of the elongating macronucleus in another heterotrich, *Blepharisma* [32]. Channels of microtubules surrounded by nuclear envelope have also been reported to pierce through the elongating macronucleus, and are aligned with the direction of macronuclear elongation [46].

A considerable amount of effort over multiple decades has been directed towards studying the macronuclear shape change cycle. The picture that developed from these studies and observations shows a complicated and regulated process. While many of the building blocks used to shape the macronucleus are familiar to biologists studying metazoan nuclei - chromatin, nucleoli, nuclear envelope, and the cytoskeleton - the forms and extreme size and time scales at which these components operate are unique to *Stentor*. The molecular mechanisms that drive these familiar components into unfamiliar shapes are completely unknown. The classical work on *Stentor's* macronucleus took place before the maturation of genetic tools and molecular biology techniques dramatically changed the field of cell biology. *Stentor's* complexity became a disadvantage as biologists moved towards organisms where developing genetic tools was more feasible.

The development of genetic and molecular tools are now revitalizing *Stentor* research. The recent sequencing of the genome, RNA-seq of gene expression, and development of RNAi in *Stentor* are now enabling us to study molecular mechanisms in *Stentor* [53] [52] [54]. Here we focus on the mechanisms that shape the macronucleus in *Stentor*.

In chapter 2, we cover the role that the nuclear transport factor, CSE1, plays in the macronuclear condensation of *Stentor coeruleus*. We measured the volume change that the

macronucleus undergoes during the macronuclear shape change cycle. We found that the volume increases while the macronucleus condenses into a single mass, and then the volume decreases as the macronucleus elongates. We looked towards the list of genes that are differentially expressed during regeneration and identified CSE1 as a potential candidate for further study. We found that when CSE1 expression is knocked down by RNAi, the macronucleus no longer condenses into a single node, and the volume increase is diminished. Over time the macronuclei are unable to maintain their beads on a string shape and the nodes become less circular. We imaged CSE1 localization using immunofluorescence, and found that CSE1 is mainly cytoplasmic early in regeneration, predominantly intranuclear in the condensed macronucleus, and then degrades at approximately the time that elongation takes place. We propose a model where CSE1 increases the flux of protein transport towards the macronucleus during condensation, causing the volume increase that is necessary to convert the macronuclear shape from moniliform to spherical.

In chapter 3, we report observations about macronuclear elongation and the transient microtubule structures that are built at this time. In transmission electron microscopy studies of *Blepharisma* and *Stentor coeruleus*, an external sheath of microtubules has been observed during macronucleuar elongation [32][47]. There is also one report of microtubule bundles encased in nuclear envelope channels piercing *Stentor's* macronucleus during elongation [46]. Here we report for the first time observations of these structures using immunofluorescence, which allows us to visualize the larger structure as opposed to a small slice of it. We also report a node shape defect in stentors fed bacteria expressing RNAi against a SUN homolog,

suggesting that the LINC complex may play a role in maintaining macronuclear shape. These observations may provide an interesting starting point for future investigations.

Chapter 2

CSE1 drives macronuclear condensation

Rebecca M. McGillivary, Pranidhi Sood, Katherine Hammar, Wallace F. Marshall

2.1 Abstract

The giant ciliate, *Stentor coeruleus*, provides a unique opportunity to study nuclear shape because its macronucleus undergoes a rapid, dramatic, and developmentally regulated shape change. During a two hour time period within cell division and regeneration, the 400 um long moniliform macronucleus condenses into a single mass, elongates into a vermiform shape, and then renodulates, returning to its original beads-on-a-string morphology [63]. Previous work from the 1960's - 1980's demonstrated that the macronuclear shape change is a highly

regulated part of cell division and regeneration, but there were no molecular studies into this process [18] [16]. With the recent availability of a sequenced *Stentor* genome, a transcriptome during regeneration, and molecular tools like RNAi, it is now possible to investigate the molecular mechanisms that drive macronuclear shape change [52] [53] [54]. We found that the volume of the macronucleus increases during condensation. When the nuclear transport factor, CSE1, is knocked down by RNAi, this volume increase is reduced, and the nodes are unable to fuse. This affects the final morphology of the macronucleus: 24 hours after regeneration the macronucleus is misshapen. We found that CSE1 is mainly cytoplasmic during interphase and in early regeneration, and then becomes mainly macronuclear during condensation. At the end of regeneration CSE1 is degraded while the macronucleus returns to its pre-condensation volume. We propose a model in which nuclear transport via CSE1 increases the volume of the macronucleus, driving the condensation of the many nodes into a single mass.

2.2 Introduction

Nuclear size and shape are among the most visible and important aspects of cell geometry. In most mammalian cell types, the nucleus is a spheroid shape and the nucleus to cytoplasm ratio is tightly controlled. Breakdown in control of nuclear size and shape is an indicator of major problems within the cell. For example, the main criteria used to diagnose and stage cancerous cells since the 1800's are defects in the size and shape of the nucleus [29]. Yet

our knowledge of the causes and consequences of these shape changes is extremely limited. In the example of cancerous cells, many components of the cell are misregulated, making it difficult to determine which changes affect nuclear structure. An alternative approach for learning how cells regulate the shapes and sizes of their nuclei is by studying cells that naturally that undergo developmentally regulated and dramatic nuclear shape changes as part of their normal physiology. A system that has a developmentally regulated shape change will allow us to more readily link changes in gene expression to alterations in nuclear shape. The more extreme the shape change, the better, because a dramatic shape change makes it easier to quantify the change and to detect subtle effects of perturbations that might be missed when the normal nuclear changes are less dramatic. Opportunities to study this have been limited by a lack of model systems. While some specific cell types in metazoans such as neutrophils or *Xenopus* epidermal tail fin cells develop lobed and branched nuclear shapes, most metazoan model systems maintain spheroid nuclei [3] [10]. There is, however, a classical model organism whose extreme and developmentally regulated shape change creates an opportunity to dissect the mechanisms of nuclear shape control: *Stentor coeruleus*.

2.3 Results

Stentor coeruleus is a giant ciliate that can extend up to 1 mm long. *Stentor* is a cone-shaped cell with a ciliated oral apparatus (OA) at the wide anterior end **(Figure 2.1 A)**. Cortical rows of microtubules and cilia run down the length of the cell to the holdfast at the posterior

end. This large and complex cell has a correspondingly large macronucleus that is 400 um in length and contains approximately 60,000 copies of its genome [53]. The macronucleus is visible without any staining due to the difference in refractive index between the cytoplasm and the macronucleus. The macronucleus appears as a string of clear beads that are about 30 um in diameter **(Figure 2.1 A)**. The many nodes of the macronucleus are continuous with each other and are connected by thin regions that are about 1-2 um wide. The nodes are contained by a single nuclear envelope, and both the nodes and the connections between them contain DNA **(Figure 2.1 B)**. Transmission electron microscopy of a node shows a double-membrane nuclear envelope surrounding chromatin, as well as multiple dark-staining areas that are consistent with *Stentor* nucleoli **(Figure 2.1 C)** [47]. Thus, while having an unusual shape, the *Stentor* macronucleus shares the same ultrastructural organization of other eukaryotic nuclei.

In addition to its remarkable shape, *Stentor's* macronucleus also undergoes a dramatic, regulated, and reversible shape change. During vegetative cell division, a new OA forms in the middle of the cell and the two daughter cells split after OA development is complete. This process happens in 8 stages that each take approximately 1 hour, the last 5 of which are illustrated in **Figure 2.2 D**. During this process, the macronuclear nodes condense into a single mass, elongate into a sausage-like shape, and then renodulate. The macronucleus does not undergo mitosis, instead it is split by the cleavage furrow between the two daughter cells as they separate [13]. This process, called the macronuclear shape-change cycle, also occurs when *Stentor* regenerates its oral apparatus after removal by cutting or by sucrose shock

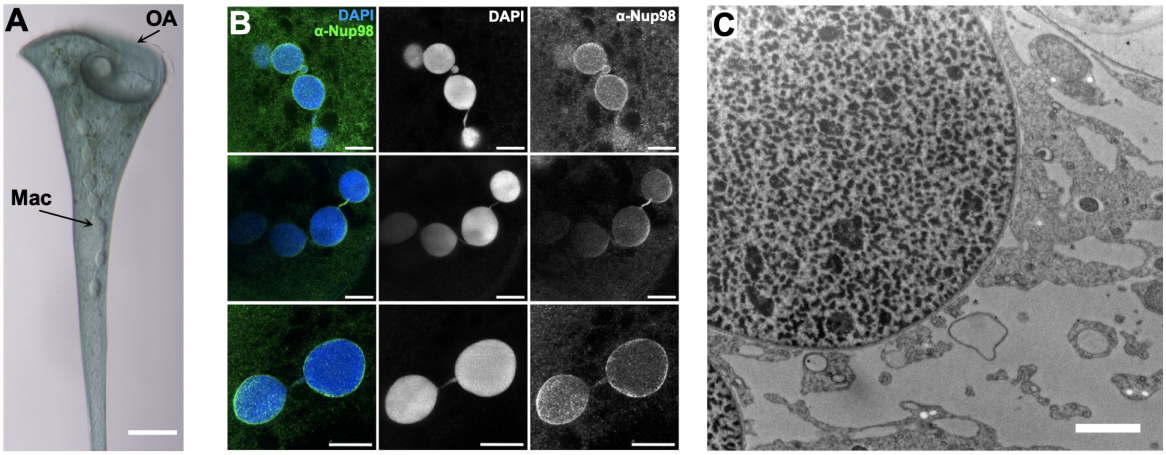

Figure 2.1: Stentor macronuclear structure. (A) Brightfield image of *Stentor coeruleus* (scale bar = 100 um). The oral apparatus (OA, arrow) curls around the anterior of the cell. The macronucleus (Mac, arrow) is visible as a moniliform series of connected nodes within the cell, resembling a string of glass beads. The macronucleus extends from the membranellar band to the beginning of the thin contractile tail. (B) Immunofluorescence images of the macronucleus in methanol-fixed cells stained with DAPI and anti-Nup98 (mab21A10) (scale bars = 20 um). DNA is present in both the nodes and the thin connecting regions between the nodes. The nuclear envelope surrounds both the nodes and the connecting regions. Images were taken with the same objective, but cropped to show regions of interest. (C) Transmission electron microscopy of the macronucleus (scale bar = 2 um). A double membrane nuclear envelope surrounds the macronuclear node. The node contains multiple large features whose staining is consistent with them being nucleoli as described in Pelvat, 1982 [47]. Chromatin density appears to vary throughout the node, with no region having denser or lighter staining than another.

[63]. This allows us to experimentally induce this nuclear shape change synchronously in a population of cells. This inducibility, coupled with the developing set of tools available in *Stentor* such as RNAi make *Stentor* an interesting system in which to study the regulation of nuclear shape change [52].

We are not the first to take note of *Stentor's* remarkable macronucleus. Previous work from the 1960's - 1980's has investigated the macronuclear shape change cycle through micro-

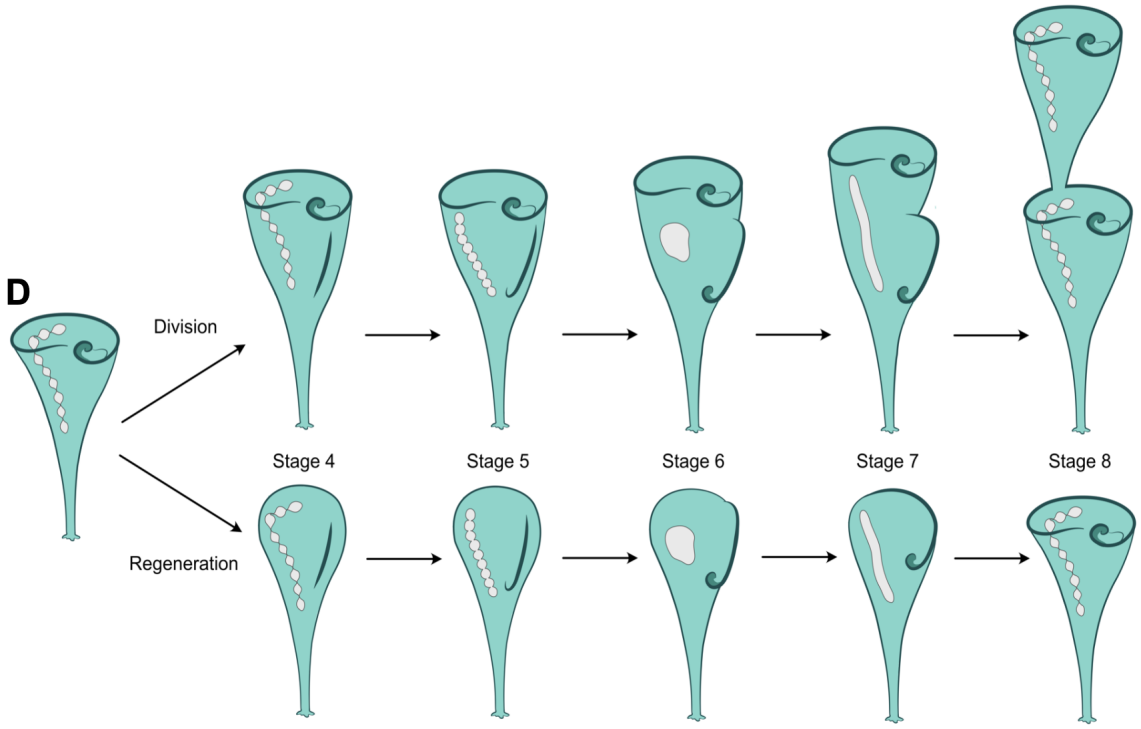

Figure 2.2: Stentor division and regeneration. (D) Diagram of the macronuclear shape-change cycle in both cell division and regeneration. *Stentor* division and regeneration has 8 morphological stages that take place over the course of 8 hours. During cell division, a new oral apparatus forms in the middle of the cell. This oral primordium elongates, curls at the posterior end to form a new oral pouch, then inserts into the cleavage furrow to form the new oral apparatus of the posterior daughter cell. During this process the thin connecting regions shorten, the macronuclear nodes come into direct contact with each other, and eventually they fuse together to produce a single compact shape. The macronucleus then elongates into a vermiform shape before renodulating back into a moniliform shape. The macronucleus is cut in two by the constriction formed between the anterior daughter cell's tail and the posterior daughter cell's frontal field. During regeneration, the oral apparatus and the macronucleus undergo the same morphological changes with the same timing as the stages of cell division.

transplantation experiments and by electron microscopy. Early studies showed that a change in the cytoplasm must cause macronuclear condensation, as evidenced by the fact that a nucleus transplanted from a non-regenerating cell into a regenerating cell will undergo the shape change [69] [63]. Macronuclei transplanted into stage 3 regenerating *Stentor* condensed more efficiently than macronuclei transplanted into stage 4 hosts - suggesting that the cytoplasmic conditions needed for condensation are present at about three hours after sucrose shock [18]. These experiments showed that the interactions between the macronucleus and cytoplasm are crucial for condensation of the macronucleus. Condensation itself involves alterations to the chromatin: electron microscopy studies show that the chromatin appears completely homogeneous by the time the macronucleus begins elongation [47]. Elongation of the macronucleus involves the microtubule cortex in addition to the cytoplasm. Electron microscopy studies have shown that a sheath of microtubules, as well as channels of microtubules piercing the macronucleus, are formed during elongation [47] [46]. Grafting experiments showed that elongation of the macronucleus is aligned with the cortical rows [16]. With the technology available at the time, previous researchers built up a picture of an extremely complex and regulated process - however virtually nothing is known about the physical or molecular nature of the macronuclear shape change process.

At a physical level, converting from a string of small spheres to a single large compact shape will entail either an increase in volume or a decrease in surface area. One simple hypothesis is that the more compact shape is achieved by increasing the nuclear volume, much like inflating a balloon. However, the dynamics of the macronuclear shape change

cycle in single *Stentor* cells have never been quantified. We therefore began by measuring the volume and node count changes that occur during the macronuclear shape change cycle. The large size and constant motion of *Stentor* cells poses a challenge for live cell imaging. We found that a traditional Shaeffer rotocompressor allows the entire macronucleus to stay in focus while shlowing the stentor's movement, yet still allowing the cell to live and regenerate. We imaged the later half of regeneration using a Zeiss Axiozoom **(Figure 2.3 E)**. We then calculated the approximate volume of the macronucleus by fitting a stack of cylinders along the midline of the macronucleus **(Supplemental Figure 2.11 A).** We found that the volume of the macronucleus dramatically increases at exactly the same time that the node count decreases during macronuclear condensation **(Figure 2.3 F).** This trend occurred for 6 of the 9 macronuclear cycles that were imaged **(Supplemental Figure 2.12 B)**. The time that the macronucleus spent in its condensed state varied, but was followed by elongation into a vermiform shape. We observed nodulation occurring simultaneously across the entire length of the macronucleus **(Figure 2.3E).**

What molecular players are driving these dramatic physical changes? De Terra previously showed that some factor is present in the cytoplasm of regenerating cells approximately 3 hours after induction of regeneration that stimulates nuclear compaction. Given the fact that Regeneration in *Stentor* is accompanied by a specific gene expression program, we hypothesized that the cytoplasmic alteration might involve induction of a gene product involved in nuclear transport. To investigate this idea, we first asked whether the macronuclear shape-change cycle is in fact dependent on gene expression during regeneration, by treating stentors

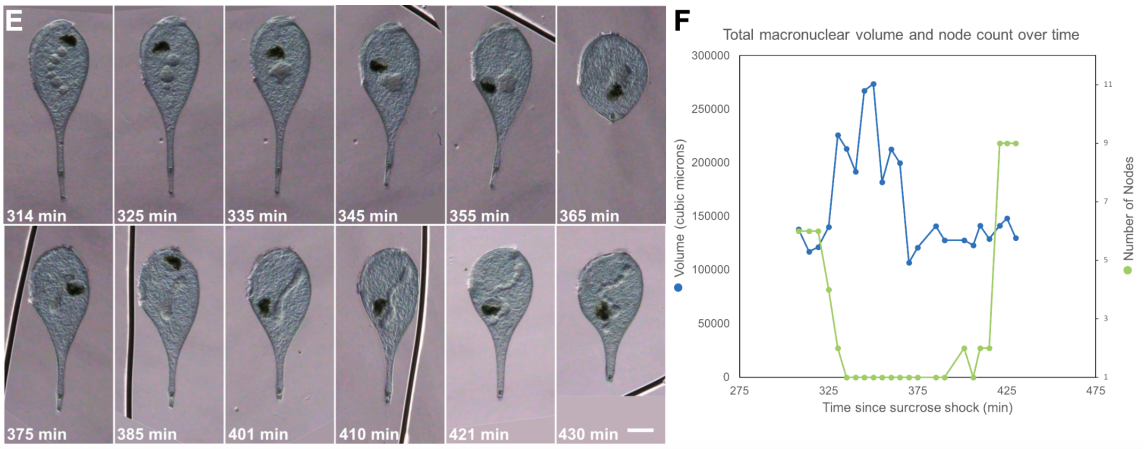

Figure 2.3: Macronuclear volume change during regeneration. (E) The macronuclear shape-change cycle observed during regeneration in a living *Stentor coeruleus* cell. The cell was immobilized and compressed in a Schaeffer rotocompressor. Scale bars = 75 um, time since sucrose shock is in the lower right corner of each image. The macronucleus condenses into a single node (t = 335 min), elongates (t = 375-401 min), and then renodulates (t = 421 min). The dark object seen in this time series is a food vacuole. (F) The total macronuclear volume was calculated by estimating the volume of a stack of cylinders along the midline of the macronucleus (Supplemental Fig S1). The number of macronuclear nodes were counted for each frame. The macronuclear volume peaks as the number of nodes decreases to one. The macronuclear volume returns to baseline as the macronucleus elongates into a vermiform shape. The macronucleus re-nodulates all at once, bringing the node count up rapidly.

with cycloheximide just after sucrose shock to prevent new protein synthesis. None of the cycloheximide treated stentors condensed their macronuclei to be under 3 nodes, while 83% of DMSO treated stentors condensed their macronuclei **(Figure 2.4 A)**, indicating that synthesis of one or more protein products during regeneration plays a role in compaction.

Next, we looked for potential candidates in the list of top differentially expressed genes during regeneration [54]. Because nuclear transport has been shown to affect overall nuclear size, [40] [37], we focused on genes encoding potential nuclear transport factors. Among the differentially expressed genes predicted to encode nuclear transport-related proteins, the gene

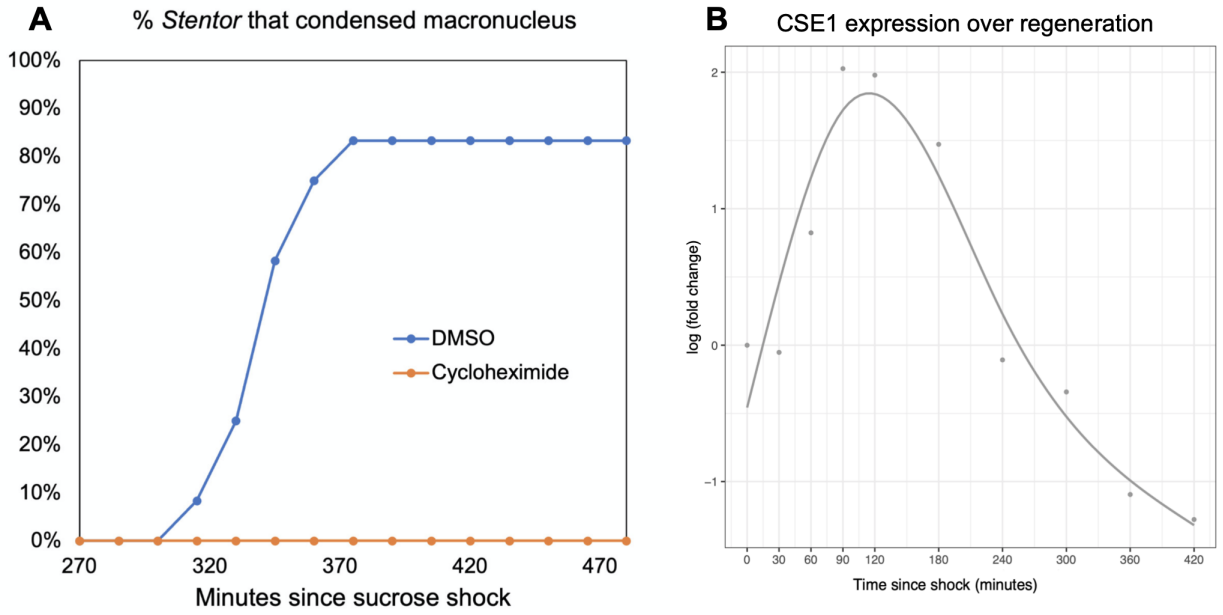

Figure 2.4: Expression of a CSE1 ortholog during macronuclear shape change. (A) Macronuclear compaction requires protein synthesis. Graph plots the percent of *Stentor* that condensed their macronucleus (defined as having 3 nodes or less) as a function of time during regeneration induced by sucrose shock. Cells were either treated with 0.01% DMSO or 5 mg/mL cycloheximide in CSW immediately after sucrose shock. 83% of cells treated with DMSO had condensed their macronucleus by 375 minutes after sucrose shock (n = 12). None of the cells treated with cycloheximide condensed their macronucleus (n = 12). (B) CSE1 expression peaks about 120 minutes after sucrose shock, increasing 2-fold relative to its expression in non-regenerating *Stentor*.

CSE1, stood out as a candidate because it is highly expressed early in regeneration before the macronuclear cycle takes place **(Figure 2.4 B)**. The peak of CSE1 expression occurs shortly before the window in which the cytoplasm is able to set up the macronucleus for its later condensation [18]. Thus, while CSE1 is expressed well before the macronuclear shape change occurs, it is expressed at exactly the expected time if it were important for macronuclear condensation. In other model systems, CSE1 is an export factor that is necessary to export importin alpha, thus making it available for the nuclear import of other proteins [30] [38].

In that sense, although technically an exportin, CSE1 is a factor whose overall function is to promote nuclear import. This candidate therefore fulfilled the requirements for our hypothetical mediator of increased macronuclear volume during *Stentor* regeneration. The predicted domain structure of *Stentor* CSE1 is similar to *S. cerevisiae* CSE1 **(Figure 2.5 C).** *Stentor* CSE1 is homologous to CSE1 in other organisms **(Figure 2.5D, Supplemental Figure 2.19).** There are two *Stentor* genes that are homologous to CSE1; these two *Stentor* genes are 92% identical to each other **(Supplemental Figure 2.19).** In the following experiments we used *Stentor* gene SteCoe_28374 to create RNAi constructs **(Table 2.1)**.

Is CSE1 necessary for volume increase and/or shape change during the macronuclear shape-change cycle? To test this, we fed *Stentor* bacteria expressing RNAi constructs directed against CSE1 for 7 days, and measured the macronuclear shape-change cycle in these cells, induced by sucrose shock. We imaged these cells for 1 hour longer than control *Stentor* to account for *CSE1(RNAi) Stentor's* slightly slowed regeneration **(Supplemental Figure 2.14 B)**. Four out of six cells showed no clear peak in volume **(Figure 2.6 A,B and Supplemental Figures 2.13 and 2.14).** CSE1 RNAi cells generally had smaller increases in volume than wild-type stentors, and reached their max volumes with a slower rate of growth than wild-type stentors **(Figure 2.7 C, D)**. All CSE1 RNAi cells were unable to compact their nucleus into less than 3 nodes - instead we observed that the nodes often bunched together, but many nodes failed to fuse **(Figure 2.7 E)**. This data shows that CSE1 is necessary for both macronuclear condensation and volume increase during the macronuclear shape-change cycle.

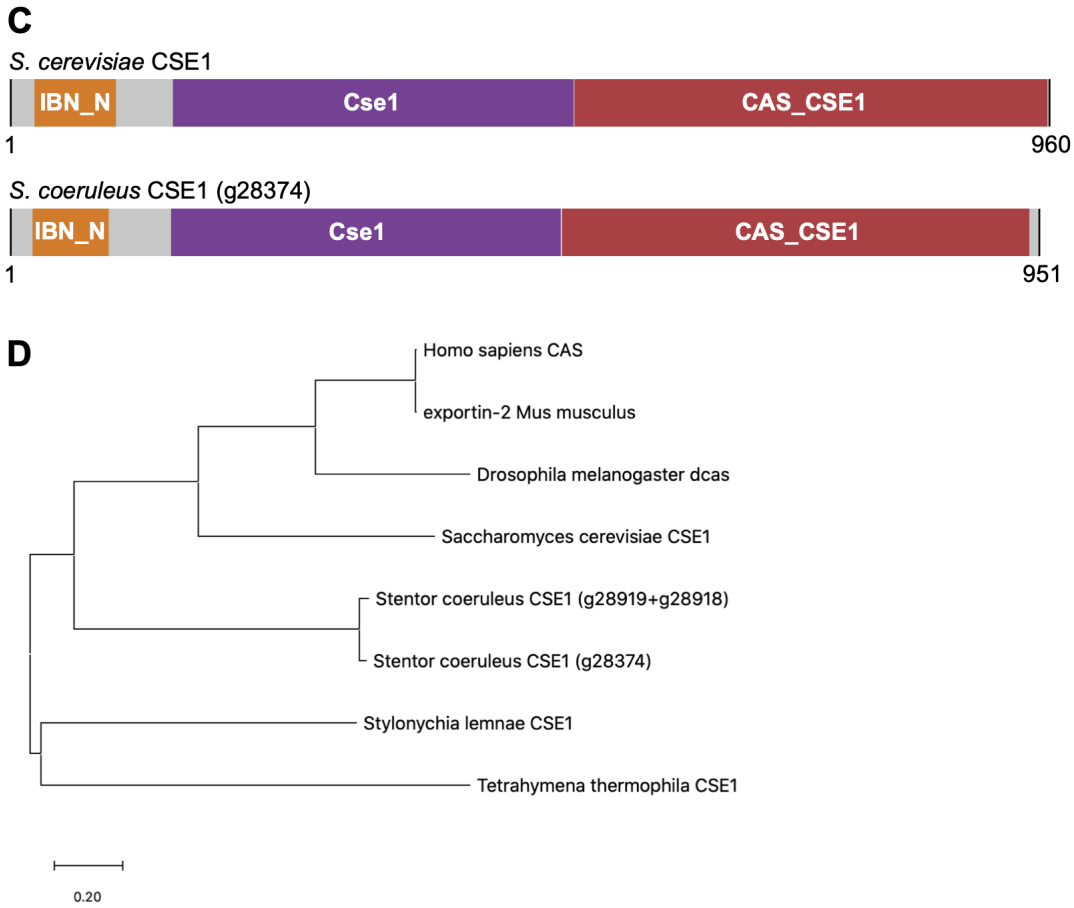

Figure 2.5: CSE1 homologs. (C) Diagram of domain structures of *S. cerevisiae* CSE1 protein and *S. coeruleus* CSE1 protein. Pfam domains were determined using InterPro. (D) Phylogenetic tree showing the two *Stentor coeruleus* CSE1 homologs and their relationship to CSE1 homologs in other organisms

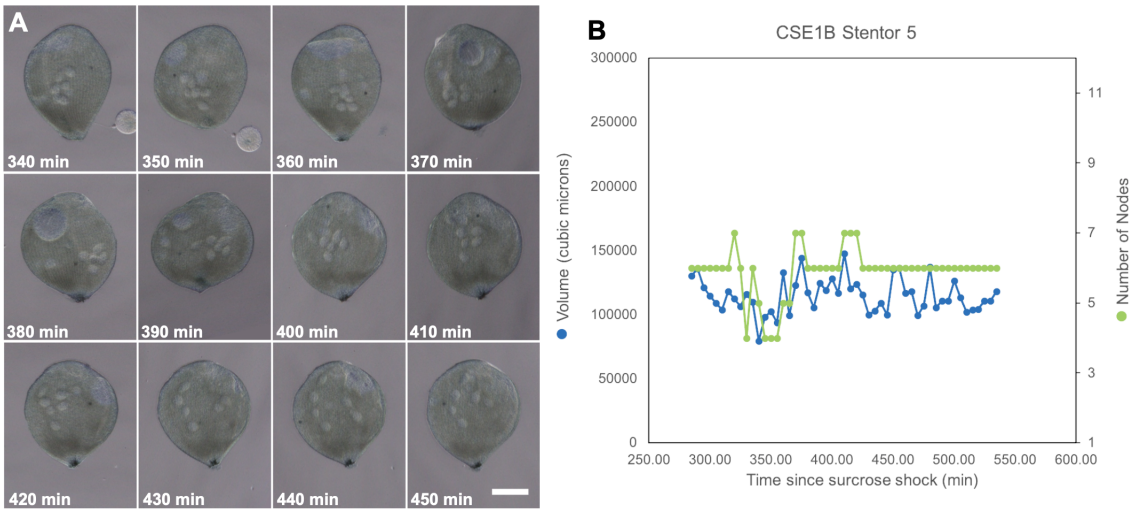

Figure 2.6: Macronuclear cycle in CSE1 RNAi *Stentor*. (A) Brightfield images of a rotocompressed *CSE1(RNAi) B Stentor* during regeneration (Scale bar = 100 um). The macronuclear nodes clump together and then spread out. The nodes never condensed into a single mass in this cell. (B) Plot showing volume and number of macronuclear nodes over time after sucrose shock. This *CSE1(RNAi) B Stentor* did not show a peak in macronuclear volume during regeneration. The node count starts at 6 nodes, decreases slightly to 4 nodes, and then returns to 6 nodes.

The physiological impact of differences in nuclear shape remains poorly understood. Does the cell care what shape its nucleus is? Given the shape phenotype we observed with RNAi knockdown of CSE1, we can now ask: what are the consequences of the macronucleus failing to undergo its normal shape-change cycle due to a lack of CSE1? We imaged macronuclear structure 24 hours post-sucrose shock. Control RNAi cells had mostly circular macronuclear nodes, with an average circularity of 0.74 **(Figure 2.8 F).** We knocked down CSE1 with two non-overlapping RNAi constructs: CSE1 RNAi A and CSE1 RNAi B. Both RNAi constructs resulted in a wide variety of macronuclear shapes, with some macronuclei being elongated or having jagged edges **(Figure 2.8 F).** We quantified the average node circularity for each

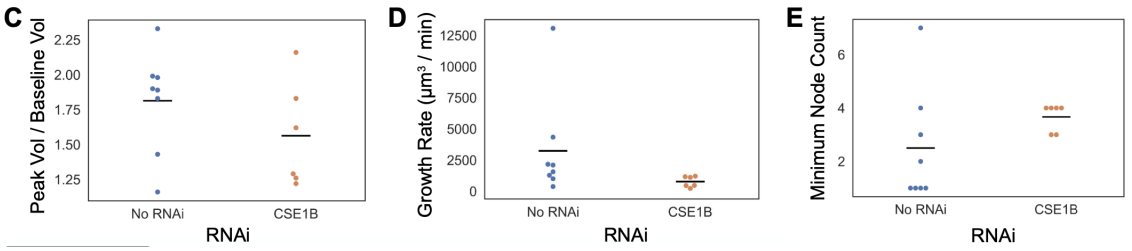

Figure 2.7: Plots comparing CSE1 RNAi and non-RNAi macronuclear cycles. (C) Plot showing the ratio between the peak volume and the baseline volume for macronuclei in regenerating *Stentor*, comparing control to CSE1 RNAi. The baseline volume was determined by visually inspecting a plot of volume versus time and estimating the average volume before compaction began. The peak volume is the maximum volume measured. For control (non-RNAi) *Stentor*, the average peak/base value is 1.81. For *CSE1 (RNAi) B Stentor*, the average peak/base value is 1.56. 1/8 non-RNAi Stentor did not show a clear peak in volume, while 4/6 *CSE1(RNAi) B Stentor* did not show a clear peak in volume (Supplemental Fig. S3) (D) Plot showing the volume growth rate of the macronucleus during condensation. Growth rate was measured as the macronuclear volume change from baseline to peak, divided by the time over which the volume change took place. Nuclear volume in non-RNAi *Stentor* grew with an average growth rate of 3,200 um3/min, with one stentor reaching a rate of 13,000 um3/min. In contrast, *CSE1(RNAi) B Stentor* averaged 780 um3/min. (E) Plot of the minimum number of nodes reached by each stentor at the point of maximal nuclear condensation. The average minimum number of nodes for Non-RNAi treated *Stentor* is 2.5, for *CSE1(RNAi) B Stentor* the average minimum node number is 3.7. 75% of Non-RNAi *Stentor* condensed their macronucleus to 3 nodes or less, while only 33% of *CSE1(RNAi) B Stentor* reached 3 nodes. None of the *CSE1(RNAi) B Stentor* were able to condense their macronuclei into a single mass.

stentor, and found that the average node circularity of *CSE1 RNAi Stentor* is significantly decreased **(Figure 2.8 G).** This indicates that the shape change cycle may be required to maintain the normal shape of the nuclear nodes. We further observed morphological changes to the overall cell shape. Wild type *Stentors* typically have elongated tails while they are undisturbed and freely swimming - we observed this in control RNAi cells. In CSE1 RNAi cells, we often observed free-swimming cells with shortened tails **(Figure 2.8 H).** These cells still had a functional holdfast and were able to contract, suggesting that while the

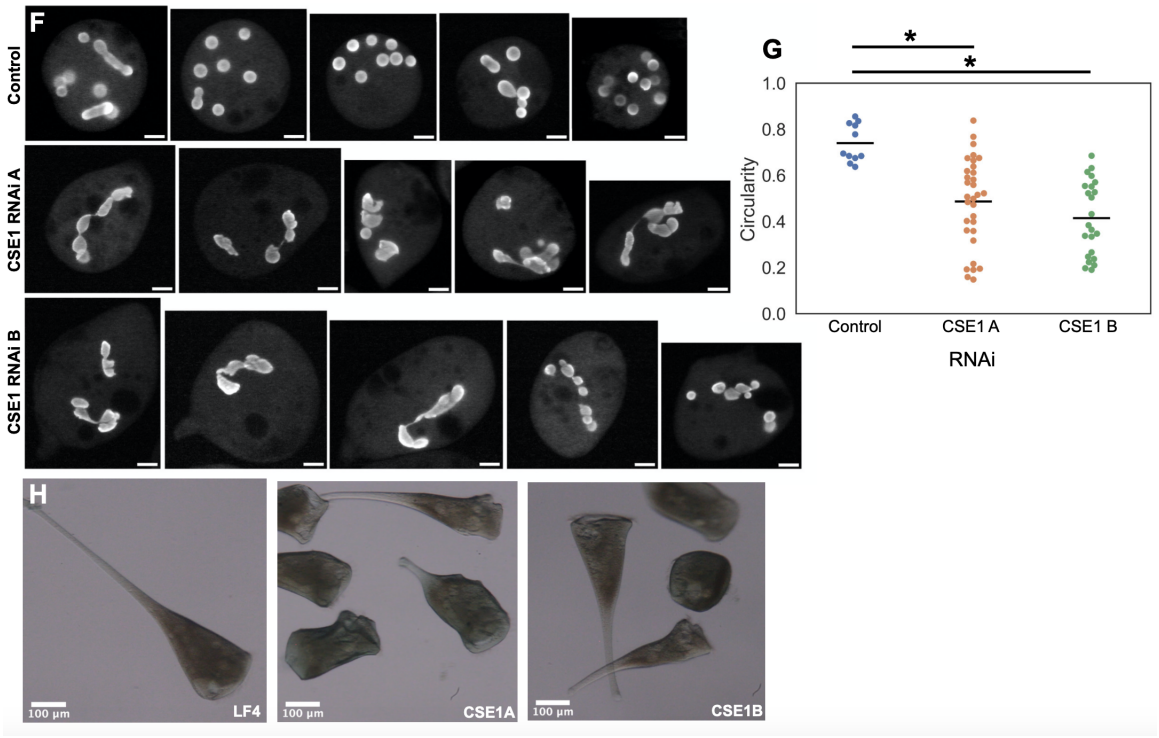

Figure 2.8: Effects of CSE1 RNAi over time. (F) Images of macronuclei 24 hours after sucrose shock (Scale bars = 50 um). Stentors were stained with Hoechst 33342 and rotocompressed. While some nodes in control (LF4 RNAi) *Stentor* are elongated, most are circular. Both *CSE1(RNAi) A* and *CSE1(RNAi) B Stentor* have irregularly shaped macronuclei, as well as a few round nodes. (G) Plot showing the average node circularity of each stentor. The average circularity is 0.74 for control *(LF4 RNAi) Stentor* (n = 11), 0.49 for *CSE1(RNAi) A Stentor* (n = 32), and 0.41 for *CSE1(RNAi) B Stentor* (n = 23). * P ¡ 0.01, Kolmogorov-Smirnov Test. (H) Brightfield images of *Stentor* after 7 days of RNAi feeding, without performing any sucrose shock (Scale bars = 100 um). Stentors with short tails are present in populations of both *CSE1(RNAi) A* and *CSE1(RNAi) B Stentor*.

proportions of the cell had changed, the components of the tail were still present.

In order to track CSE1 localization throughout regeneration, we raised a custom antibody against *Stentor* CSE1, and used a peptide block and immunofluorescence of *CSE1 RNAi Stentor* to confirm the specificity of the antibody **(Supplemental Figure 2.15 and 2.16)**. In non sucrose shocked cells, CSE1 is present in cytoplasmic puncta in both PFA- and

methanol-fixed cells **(Figure 2.9, 2.10 and Supplemental Figure 2.17).** In three cases we observed CSE1 staining become concentrated around the periphery of the macronucleus, this occurred in cells 6 hours post sucrose shock, which corresponds to the time at which macronuclei are in the process of condensing. **(Supplemental Figure 2.17).** When the macronucleus is condensed, CSE1 is present in the interior of the macronucleus **(Figure 2.9).** This occurs in both PFA-fixed stentors that have been permeabilized with Triton-X100, as well as methanol-fixed stentors, showing that the intranuclear punctate signal is not an artifact of fixation conditions **(Supplemental Figure 2.17).** Both fixation conditions show that CSE1 is dynamically re-localizing from being mainly cytoplasmic, to mainly intranuclear as the macronucleus condenses. We have also observed this in stentors undergoing cell division, suggesting that this localization change is a part of the macronuclear shape-change cycle, and not a stress response to sucrose shock **(Supplemental Figure 2.18).** In the course of these observations, we noted that by 7 hours into regeneration, CSE1 signal is dramatically reduced **(Figure 2.9, 2.10 and Supplemental Figure 2.17).** This occurs at roughly the time at which the macronucleus begins to elongate and decrease in volume.

2.4 Discussion

Early work on *Stentor* showed that there is a complex interplay between the cytoplasm, the microtubule cortex, and the macronucleus during its shape change cycle. Macronuclei are dependent on unidentified components in the cytoplasm present at particular stages in

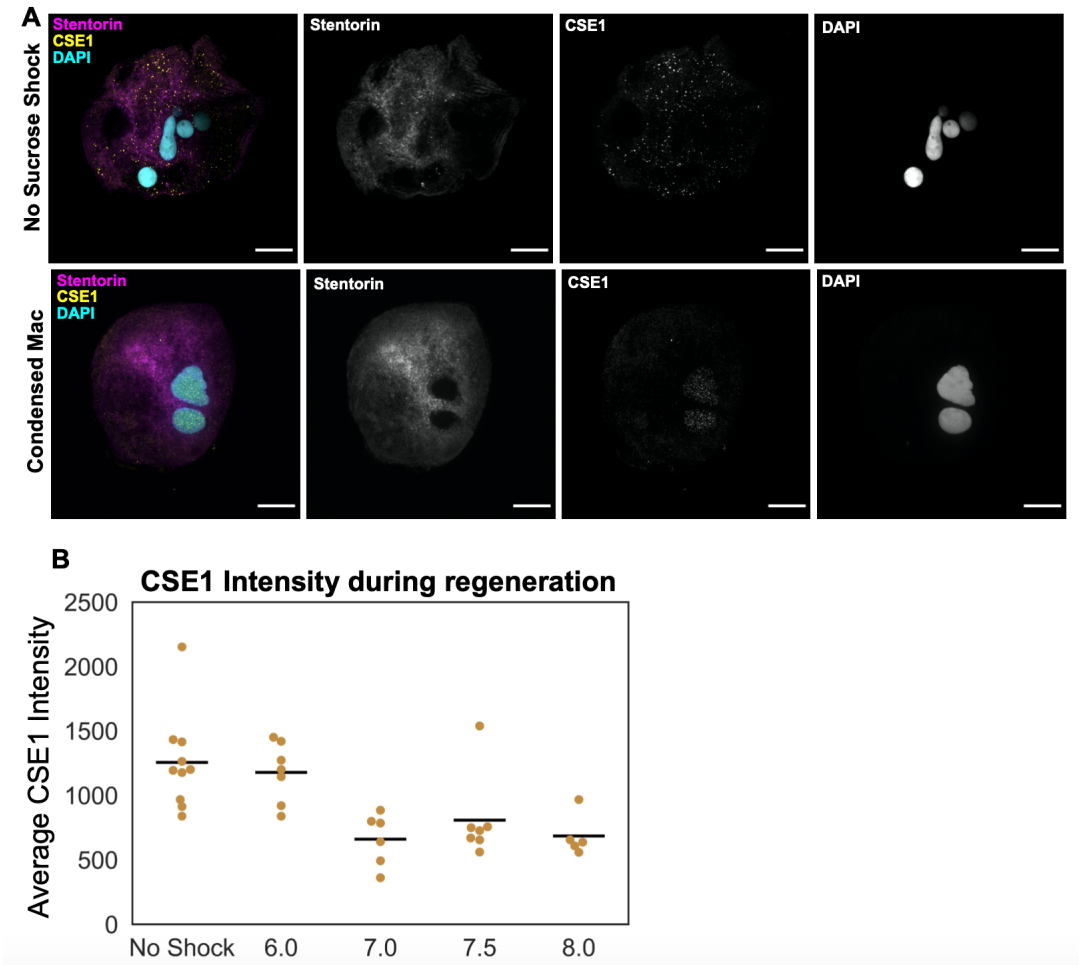

Figure 2.9: Dynamic relocalization of CSE1 during nuclear shape change. (A) Immunofluorescence images of *Stentor* showing the localization of CSE1 (scale bars = 50 um). Stentors were fixed with paraformaldehyde, stained with antibodies against CSE1 as well as DAPI to detect DNA, and imaged on a spinning disk confocal microscope. The cytoplasm was visualized by imaging autofluorescence generated by the blue pigment stentorin. In cells that have not been sucrose shocked, CSE1 is present in cytoplasmic puncta, with little staining present inside the macronucleus. In cells with condensed macronuclei during regeneration, CSE1 is present in intranuclear puncta, while cytoplasmic staining is decreased. (B) Average CSE1 intensity per cell. Stentors were fixed in methanol and CSE1 immunofluorescence was performed. All cells were imaged with the same light intensity and exposure settings. The average intensity of CSE1 staining, expressed in arbitrary units, was measured for each cell imaged. The signal from stentorin was used to define the area of the cell – the average CSE1 intensity over this area was measured. Non-shocked cells had an average CSE1 intensity of 1255, and cells 6 hours after sucrose shock had a similar CSE1 intensity of 1177. At 7 hours the average intensity drops by approximately half to 660 and remains low until the end of regeneration. The average intensity at 7.5 hours is 807, and at 8 hours it averages 685.

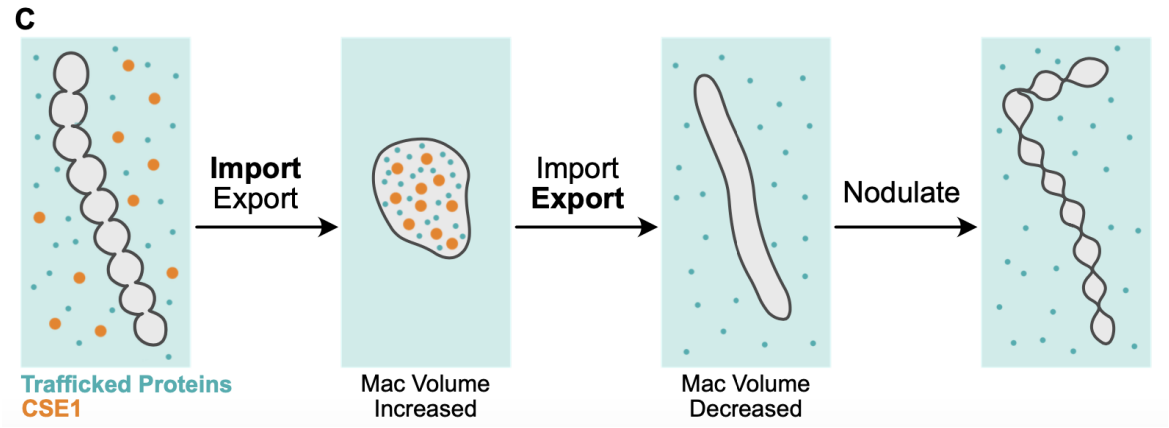

Figure 2.10: Model of CSE1's role in macronuclear condensation. (C) Model for how CSE1 may be promoting macronuclear condensation and volume increase. Nuclear proteins imported and exported from the macronucleus are represented by small blue dots – the exact identities of these proteins are currently unknown. CSE1 is represented by larger orange dots. The cytoplasm is light blue while the nucleoplasm is light gray. Before condensation, CSE1 and many proteins are cytoplasmic. We hypothesize that during compaction, nuclear import increases. This increased transport increases the amount of proteins inside the macronucleus, which in turn leads to the volume increases and causes the macronucleus to condense into a single mass to accommodate this change in surface to volume ratio. CSE1 is localized mainly to the nucleoplasm at the stage of high compaction. Shortly after condensation, CSE1 protein levels begin to drop, causing nuclear transport to shift towards nuclear export, such that the macronuclear volume decreases, and the macronucleus can achieve an elongated shape. At the end of the macronuclear cycle the macronucleus nodulates and CSE1 degradation is complete.

order to progress into the next stage of the cycle, and the structural components of the macronucleus itself change dramatically throughout the cycle. The macronuclear shape change cycle consists of many different processes occurring over three phases: 1. the fusion of the nodes coupled with their migration towards the center of the cell and a near-doubling of the nuclear volume; 2. the condensed macronucleus reducing its volume to baseline and elongating along microtubule structures; and 3. the elongated macronucleus rapidly re-nodulating along its entire length. In this paper we have identified the first molecular

component involved in the regulation of macronuclear shape change: CSE1.

CSE1 is necessary for the fusion of nodes and the volume increase that occurs during phase 1 of the macronuclear shape change cycle. We have shown that when stentors are treated with CSE1 RNAi, the macronuclear condensation is defective - the nodes do not fuse to the same extent as wild type, the volume increases less, and the rate at which the macronucleus increases in volume is reduced. We also observed that, in CSE1 RNAi cells, the nodes still appear to migrate towards each other, suggesting that some other factor is driving the positioning of the nodes.

How might CSE1 be driving the volume increase of the macronucleus? Alterations in nucleocytoplasmic transport of proteins have been shown to affect the volume of nuclei in metazoan cells. While some studies suggest overall flux of proteins into the nucleus can increase volume, the import of lamins is especially effective at facilitating nuclear volume increase [40] [37] [8]. *Stentor*, like all ciliates, has no genes that are homologous to lamins. Further investigation into the structure and composition of *Stentor's* nuclear envelope are needed to determine if there are some proteins that play a similar role as lamins do in metazoans.

While it is unclear exactly which proteins are trafficked into the macronucleus during condensation, CSE1 likely plays a role in their import. In other systems, CSE1 keeps the cycle of nuclear import running by exporting importin alpha out of the nucleus, ensuring importin alpha is available in the cytoplasm to import more proteins into the nucleus. When CSE1 levels are depleted in *S. cerevisiae*, importin alpha is sequestered inside the nucleus

[30]. In *Drosophila*, the CSE1 homolog dcas switches from a predominantly cytoplasmic to a nuclear localization at different stages of oogenesis [64]. This redistribution of CSE1 in *Drosophila* is thought to reflect changes in nuclear transport, given that stages with high amounts of nuclear dcas correspond to stages in which the overall protein levels of the nucleus are increased [64]. In *Stentor,* the re-localization of CSE1 from the cytoplasm to the macronucleus during condensation suggests that a similar shift in the overall direction of nuclear transport towards the macronucleus has taken place **(Figure 4A)**. Degradation of CSE1 protein after condensation could be causing a decrease in nuclear import, allowing the macronucleus to decrease in volume. Overall, the picture emerges of *Stentor* transiently increasing its levels of CSE1 in order to drive more import of material into the macronucleus during the compaction phase of the nuclear shape change **(Figure 2.10 C).**

Besides an increase in volume, the other notable aspect of the macronuclear shape change cycle is the fusion of the nodes. The fusion may simply be a direct physical result of this volume increase. Node fusion does not require any membrane fusion, as the nodes are, from the beginning, linked by thin regions and are contained within a single nuclear envelope. Nodes that have been severed from each other cannot fuse [15]. If the volume increase outpaces an increase in nuclear surface area, then the beads on a chain shape cannot be maintained. The macronucleus would more and more begin to resemble the shape with the maximum volume:surface area ratio: a sphere. If CSE1 cells are unable to increase their volume as much as wild type, then the most energetically favorable path would be to remain in a moniliform shape, or to have incomplete node fusion. Altering the nuclear shape may

be a common way to accommodate alterations in the surface area:volume ratio of nuclei; some sec mutant *S. cerevisiae* cells have their nuclear envelope growth outpace the growth of their nuclear volume, and develop bilobed nuclei as a result [65].

How might *Stentor* benefit from undergoing the macronuclear shape change cycle? One feature that separates *Stentor's* macronuclear shape change cycle from other models in metazoans is the reversibility of the change - *Stentor's* macronucleus completes the process looking similar to how it began, albeit with a slightly increased number of nodes. Because of this, the purpose of the macronuclear shape change cycle has been unclear. A variety of competing hypotheses have been proposed for why *Stentor* would compact its nucleus during division, ranging from the idea that it makes it easier to split during cytokinesis, to the hypothesis that it allows *Stentor* to rapidly increase its number of nodes [63]. No consensus has been reached on this matter. It was interesting to note, then, that *CSE1 RNAi Stentor*, in addition to failing to compact fully, were unable to re-establish a normal moniliform shape after regeneration was complete. This suggests that condensing the macronucleus is important for maintaining its normal shape. Biophysical measurements of membrane tension and nucleoplasmic density before, during, and after macronuclear condensation would help us understand how the macronuclear shape change cycle helps maintain the moniliform shape of *Stentor* during interphase.

We also observed that some *CSE1 RNAi Stentor* appeared to have shortened posterior halves after 7 days of RNAi feeding **(Figure 2.8 H)**. It is plausible that the misshapen macronucleus of *CSE1 RNAi Stentor* is unable to extend the length of the cell to properly

distribute mRNA throughout the entire cytoplasm, and the posterior half begins to shrink as a result. In other species of *Stentor*, the macronuclear shape usually corresponds to the size of the cell. The smallest species, like *Stentor multiformis*, have spherical macronuclei. Intermediate species like *Stentor roseli* have vermiform macronuclei. *Stentor coeruleus* is one of the largest *Stentor* species, and like other giant heterotrich ciliates like *Spirostomum*, it has a beaded macronucleus [63]. This shape of nucleus could be useful for stretching the macronucleus across long distances in giant ciliates, thus providing a local source of message for different regions of the cell. The misshapen macronuclei of CSE1 RNAi cells may be unable to efficiently reach across the length of *Stentor* needed to support the maintenance of all of its cellular structures.

Giant and syncytial cells in fungi and animals often have many nuclei that are distributed throughout the cell, and these distributions are important for the cells to function properly. In muscle fibers, the nuclei are located at the periphery of the fiber, and spaced such that the distance between them is maximized [9]. In various muscle diseases, and also during muscle repair, the nuclei are often clustered in the center of the muscle fiber [21] [49]. The hyphae of fungi like *Ashbya gossypii* also have multiple nuclei distributed along their lengths [19] [26]. In mutant strains of *Ashbya* where nuclei are randomly spaced, nuclei that are clustered together undergo mitosis at similar times - disrupting the cell cycle independence of each nucleus within the hyphae [2]. When cells reach large size scales, regulating the distribution of nuclear material is important for maintaining the overall cellular architecture.

The macronucleus of *Stentor coeruleus* undergoes a rapid and dramatic nuclear shape

change that has long fascinated cell biologists. We have now identified the first molecular player in this shape change: CSE1. This nuclear transport factor is necessary for node condensation and volume increase to occur, and its re-localization and degradation correspond to the morphological changes of the macronucleus. The macronuclear shape change cycle is a complex process, and further understanding it will require studying more genes and investigating the physical changes that happen to the macronucleus throughout this cycle.

2.5 Methods

Stentor Strains and culturing. All RNAi, immunofluorescence, and live imaging experiments were carried out with *Stentor coeruleus* originally obtained from Carolina Biological Supply Company (Burlington, NC) and cultured in the lab. Images in figures 1A and 1C were taken of wild *Stentor coeruleus* that were obtained from North Lake in Golden Gate Park, San Francisco, CA and then cultured in the lab. *Stentor* were cultured using the same protocol detailed in Lin, 2018 [41].

Live Imaging of Macronuclear Shape Change Cycle. *Stentors* were sucrose shocked in a 15% sucrose in Carolina Spring Water (CSW) solution (Carolina Biological Supply) for two minutes. The shock was halted by rapidly diluting 2 mL of shocked stentors into 50 mL of CSW. Cells were incubated at room temperature for 4-5 hours. Stentors were then loaded into a Schaeffer rotocompressor (Biological Institute of Philadelpiha, Philadelphia PA) and compressed until their movement was just halted. Although not used for the

imaging reported here, we have also found that the Janetopolous rotocompressor (Invivo-Imaging.com) also works well to compress *Stentor* [72]. The rotocompressed stentors were then imaged using a Zeiss Axiozoom V16 equipped with a Nikon Rebel T3i SLR Camera. Timelapse images were taken every 5 minutes either manually or automatically using DSLR Remote Pro (Breeze Systems Ltd., Camberly, Surrey, UK).

Volume Calculations. The edges of the macronuclear nodes were manually traced on a transparent layer above each stentor image using the pen tool in Affinity Designer 1.9.3 (Affinity.serif.com, Serif (Europe) Ltd., Nottingham, UK). Each outline was saved as a PNG with transparent background. In FIJI each outline was filled in and converted to a binary image using a custom FIJI macro [51]. The binary images were loaded into Affinity Designer 1.9.3, and, using the lasso tool, the nodes were manually arranged so that the midline of the macronucleus was horizontal. The horizontal images were opened in FIJI and each image was cropped and converted to binary to be prepped for further analysis with Python. The python-ready images were then analyzed in a Jupyter notebook to calculate the volume of the macronucleus at each timepoint by assuming rotational symmetry around the horizontal axis of each node [34] [28] [48] [31] [66]. Details of the calculation are provided in **Supplemental Figure 2.11 A**. The number of nodes for each timepoint was visually counted from the outline images.

Phylogenetic Analysis. CSE1 homologs were identified using BLASTp [1]. CSE1 amino acid sequences were uploaded into MEGAX and aligned using MUSCLE [33] [36] [56]. Phylogenetic trees were generated using the Maximum Likelihood Method [27]. Domains of

Stentor CSE1 were identified using InterPro [5].

Cloning. Genes were amplified with PCR from genomic DNA extracted from *Stentor* using a DNeasy Blood and Tissue Kit: Animal Blood Spin-Column Protocol (QIAGEN, Germantown, MD). Genes were inserted into a pPR-T4P plasmid using ligation independent cloning [4]. The resulting vectors were then transformed into HT115 E. coli. The two CSE1 RNAi constructs target non-overlapping regions of the CSE1 gene. CSE1 RNAi A encompasses DNA bases 1247-2084, while CSE1 RNAi B targets 2089-2841. Primer sequences are listed in **Table 2.1**.

RNAi. HT115 bacteria containing the RNAi constructs were grown to OD600 0.4-0.6, and then induced with 1 mM IPTG. Induction took place for either 4 hours at 37°C or overnight at room temperature. Stentors were added to fresh CSW and fed RNAi daily for 7 days.

Hoechst Staining. Stentors were incubated in 10 ug/mL Hoechst 33342 diluted in CSW for 30 minutes. Cells were then transferred to CSW and incubated for another 30 minutes. Stentors were compressed in a rotocompressor to image the macronucleus.

Macronuclear Shape Analysis. Images of macronuclear nodes were thresholded in FIJI [51], and the circularity of each node was measured. For each stentor with multiple nodes, the circularity of the nodes were averaged together. Thus the circularity reported in each datapoint in Figure 3 is the average node circularity per *Stentor*. This ensures that cells with many nodes do not overpower cells with fewer nodes when determining the overall circularity of each population of *Stentor*.

CSE1 Antibody Generation. Pre-immune bleeds from rabbits were first screened in order to avoid using any rabbits that already produce antibodies that react with *Stentor* proteins in immunofluorescence and in western blots. This was done by incubating either fixed stentors or western blot membranes with pre-immune rabbit serum diluted at a 1:500 ratio, then staining with secondary antibodies. A custom anti-CSE1 antibody was generated using the peptide MVDFTSIFTKC (Bethyl Laboratories, Montgomery, TX). A column for affinity purification was prepared by binding the peptide to a SulfoLink resin column using the SulfoLink Immobilization Kit (Thermo Fisher). Antibodies were affinity-purified from serum using this column.

Immunofluorescence with PFA Fixation. Cells were fixed in 2% paraformaldehyde in 0.5x PBS at 4°C overnight. Cells were then rinsed in TBS and then permeabilized in 0.5% Triton X-100 in TBS. Cells were then rinsed in 0.1% Triton X-100 in TBS and blocked in 2% BSA, 0.1% Sodium Azide in TBS for 1 hour at room temperature. Primary and secondary antibodies were incubated with fixed stentors for 1 hour each at room temperature. Primary antibodies used in this study are Anti-Nup98 (mab21A10, Abcam, Waltham, MA) and a custom-generated CSE1 antibody. Secondary antibodies used in this study are Alexa-488 goat-anti-rabbit (AB_2576217, Thermo Fisher Scientific, Waltham, MA) and Alexa-488 goat–anti-mouse (Life Technologies, Grand Island, NY). Anti-Rabbit Cells were washed three times with 0.1% Triton-X100 in TBS after both antibody incubations. Cells were then placed into mounting medium (80% glycerol, 1% DMSO in 50 mM Tris pH 8.0). Slides were prepared using 0.25 mm silicone spacers in between the coverglass and slide.

Peptide Block. *Stentor* anti-CSE1 antibody and the peptide used to generate this antibody (MVDFTSIFTKC) were mixed at a 1:10 antibody:peptide molar ratio and incubated for 2 hours at room temperature.

Immunofluorescence with Methanol Fixation. Cells were fixed in -20°C methanol for either 1 hour or overnight. Cells were rinsed with 1:1 PBS:Methanol, and then again with PBS. Cells were blocked with 2% BSA in PBS for 1 hour at room temperature. Primary and secondary antibodies were incubated with stentors for 1 hour at room temperature each. Cells were rinsed with PBS and then mounted in Vectashield mounting medium. Slides were prepared using 0.25 mm silicone spacers in between the coverglass and slide.

Fluorescence Imaging. Stentors were imaged with a DeltaVision deconvolution microscope with a 20x air objective and a CoolSnap HQ camera. Z-stacks were taken with 2 um step sizes. This microscope was controlled using SoftWorx (Applied Precision). Stentors were also imaged on a Nikon Ti microscope equipped with an Andor Borealis CSU-W1 spinning disk confocal, an Andor Zyla 4.2 sCMOS camera, and a Plan Fluor 40x/1.3 oil immersion objective. This microscope was controlled using Micro-manager software [20]. Nuclear envelope immunofluorescence images were taken on a Zeiss LSM980 Airyscan confocal microscope equipped with a C-Apochromat 40x/1.20 water immersion Korr objective.

CSE1 Average Intensity Measurements. Image stacks of *Stentor* were converted into max projections. The autofluorescence of *Stentor's* pigment stripes was used to define the boundary of the cell: this channel was thresholded and converted to a binary image in FIJI. The boundary of this binary image was transferred to the CSE1 channel image, and the

average CSE1 fluorescence intensity within this boundary was measured.

Transmission Electron Microscopy. Stentors were starved such that the cytoplasm was free of visible food vacuoles and the macronucleus was clearly visible under a dissecting microscope. The fixation protocol is derived from Wloga 2008 [70]. 50 stentors were washed with 10 mM Tris-HCl pH 7.4. Immediately after the rinse, stentors were fixed for 1 hour in ice-cold 1% osmic acid, 1.5% glutaraldehyde, 25 mM cacodylate buffer pH 7.4. After fixation, the stentors were rinsed overnight at 4C in 50 mM cacodylate buffer pH 7.4. The stentors were then embedded in agar blocks, dehydrated in ethanol series, and embedded in Durcupan. Reynolds lead citrate and uranyl acetate were used to contrast the ultrathin sections. Stentors were imaged on a Zeiss 10CA transmission electron microscope.

2.6 Supplementary Figures

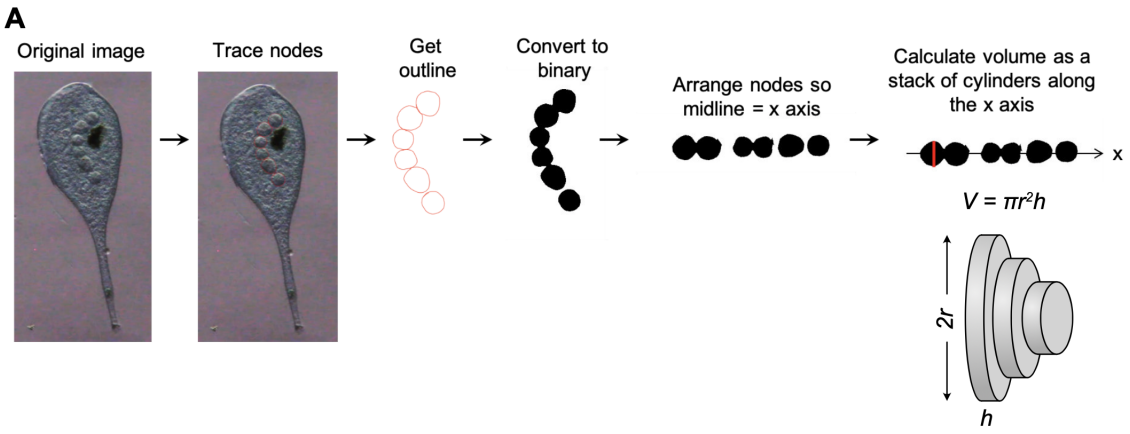

Figure 2.11: Macronuclear volume calculation pipeline. (A) Diagram of macronuclear volume calculation workflow. The macronuclear nodes are traced by hand. The traced outline is then separated from the image and filled in to create a binary image of the macronucleus. Then, the macronucleus image is split up so that the midline of the macronucleus is now a horizontal line along the x axis. The volume of the macronucleus is calculated by assuming rotational symmetry around the x axis to generate a series of cylinders of radius equal to that of the macronucleus relative to the axis at that position, and then adding up the volumes of cylinders along the macronucleus. The height of each cylinder is 1 pixel length along the x axis, and the diameter of each cylinder is the thickness of the macronucleus at that point. The red line illustrates the side view of one of these cylinders. The volume for each cylinder is calculated and added together to get the total macronuclear volume.

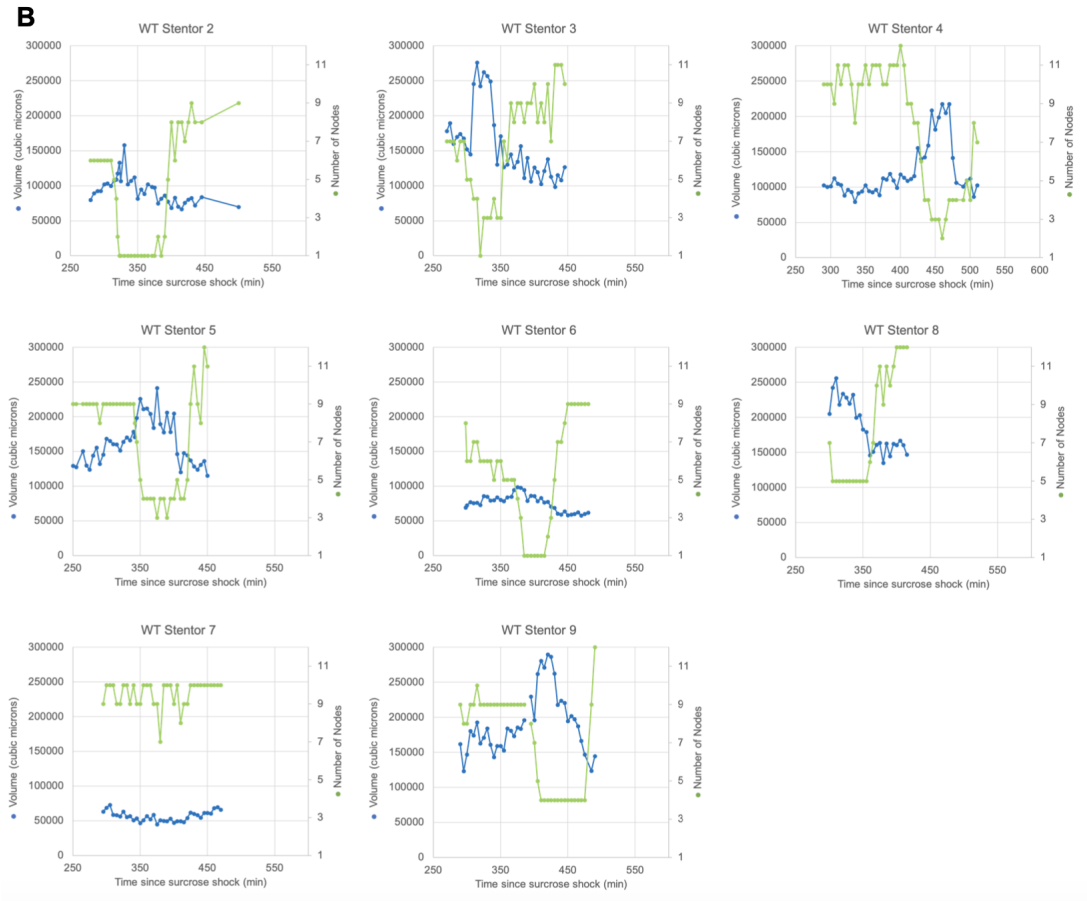

Figure 2.12: Macronuclear volume during regeneration of non-RNAi *Stentor*. (B) Plots of WT *Stentor* volume and node number changes during regeneration that were not included in Fig 1. Stentor 8 was omitted from later data analysis because a pre-condensation baseline could not be determined. In general, the macronuclear volume peaks as the node number drops, indicating that macronuclear condensation is linked to an increase in macronuclear volume.

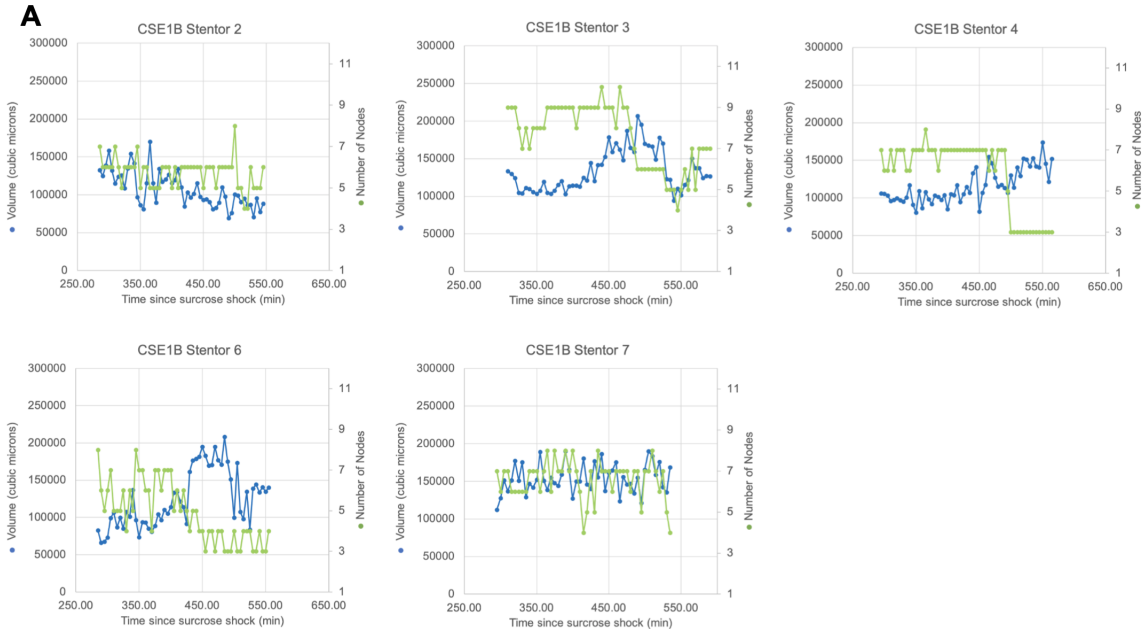

Figure 2.13: Macronuclear volume during regeneration of (*CSE1)RNAi Stentor.*(A) Plots of *CSE1(RNAi) B Stentor* volume and node number changes during regeneration from additional examples that were not shown in Fig 3. Most stentors do not have any clear peak in volume. While node count slightly decreases in some cells, a node count below 3 was never observed.

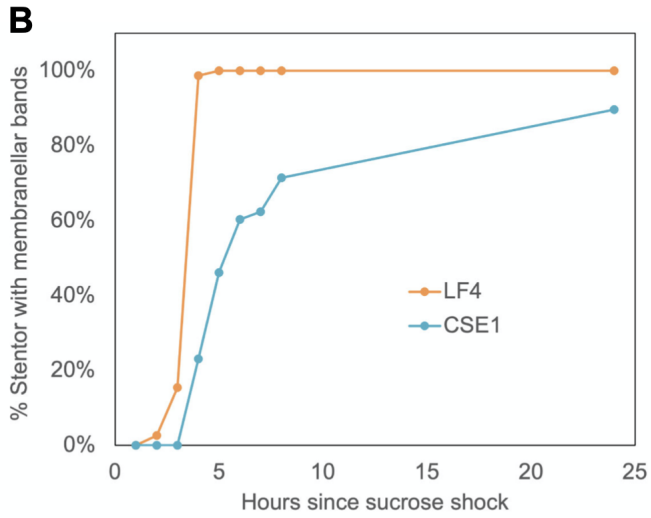

Figure 2.14: Regeneration of *CSE1(RNAi) Stentor*. (B) Plot showing the percentage of stentors that re-grew membranellar bands at various times after sucrose shock. *LF4 (control RNAi) Stentor* show a pronounced jump to 100% re-grown membranellar bands (stage 4 of regeneration) at about 4 hours (n = 77) consistent with the normal timing of regeneration. *CSE1(RNAi) A Stentor* show a lag in membranellar band regeneration, requiring more than 5 hours for half the cells to show a membranellar band. By 24 hours, 90% of cells grew a membranellar band (n = 77). This potential slowing of overall regeneration is the reason that the CSE1(RNAi) A macronuclear cycle experiments in Supplemental Figure S2A were carried out for 1 hour longer than in WT Stentor.

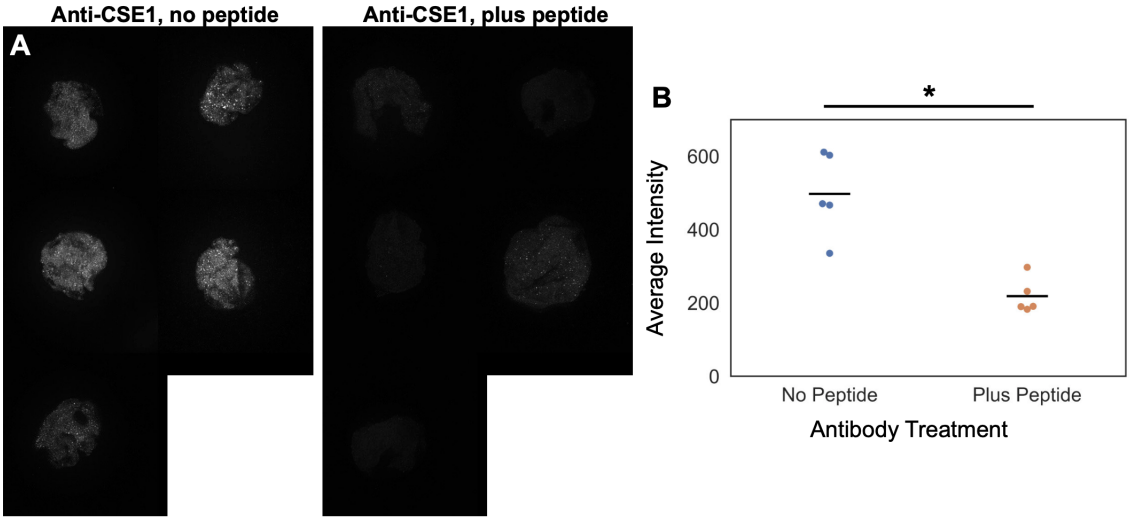

Figure 2.15: Peptide block of anti-CSE1 antibody. (A) Peptide blocking control. Images of PFA fixed *Stentor* stained with anti-CSE1 either without or with pre-incubation with CSE1 peptide. Cells were imaged with a W1 spinning disk confocal. (B) Plot showing the average CSE1 staining intensity in PFA fixed *Stentor* when the CSE1 antibody is either on its own or pre-incubated with CSE1 peptide. Without the peptide block, the average CSE1 intensity is 497 (n = 5). With peptide blocking the average CSE1 intensity drops in half to 218. *P ¡ 0.01, Two-tailed T-Test.

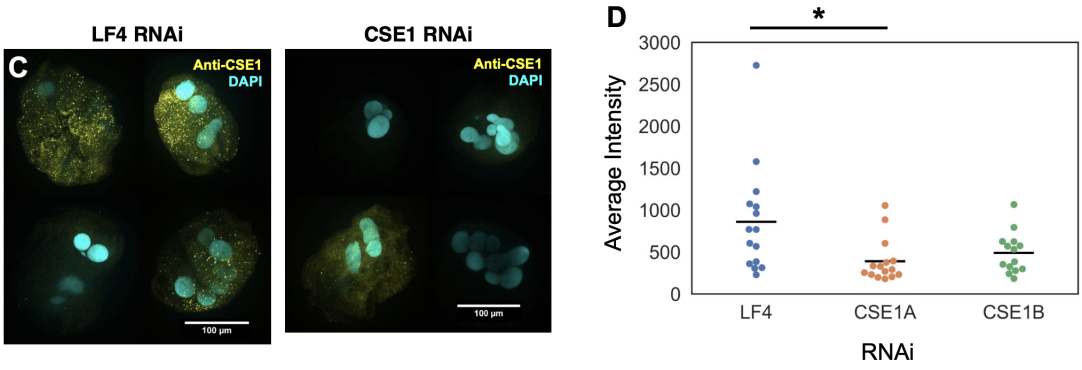

Figure 2.16: RNAi control for antibody specificity. (C) Images of PFA fixed *LF4(RNAi)* or *CSE1(RNAi) Stentor* stained with anti-CSE1. Cells were imaged with a W1 spinning disk confocal. (D) Plot showing the average CSE1 staining intensity in PFA fixed *Stentor* treated with RNAi. In *LF4(RNAi) Stentor*, the average intensity is 860. In *CSE1(RNAi) A Stentor*, the average intensity is 388. The average intensity of *CSE1(RNAi) B Stentor* is 489. *P ¡ 0.05, Two-tailed T Test.

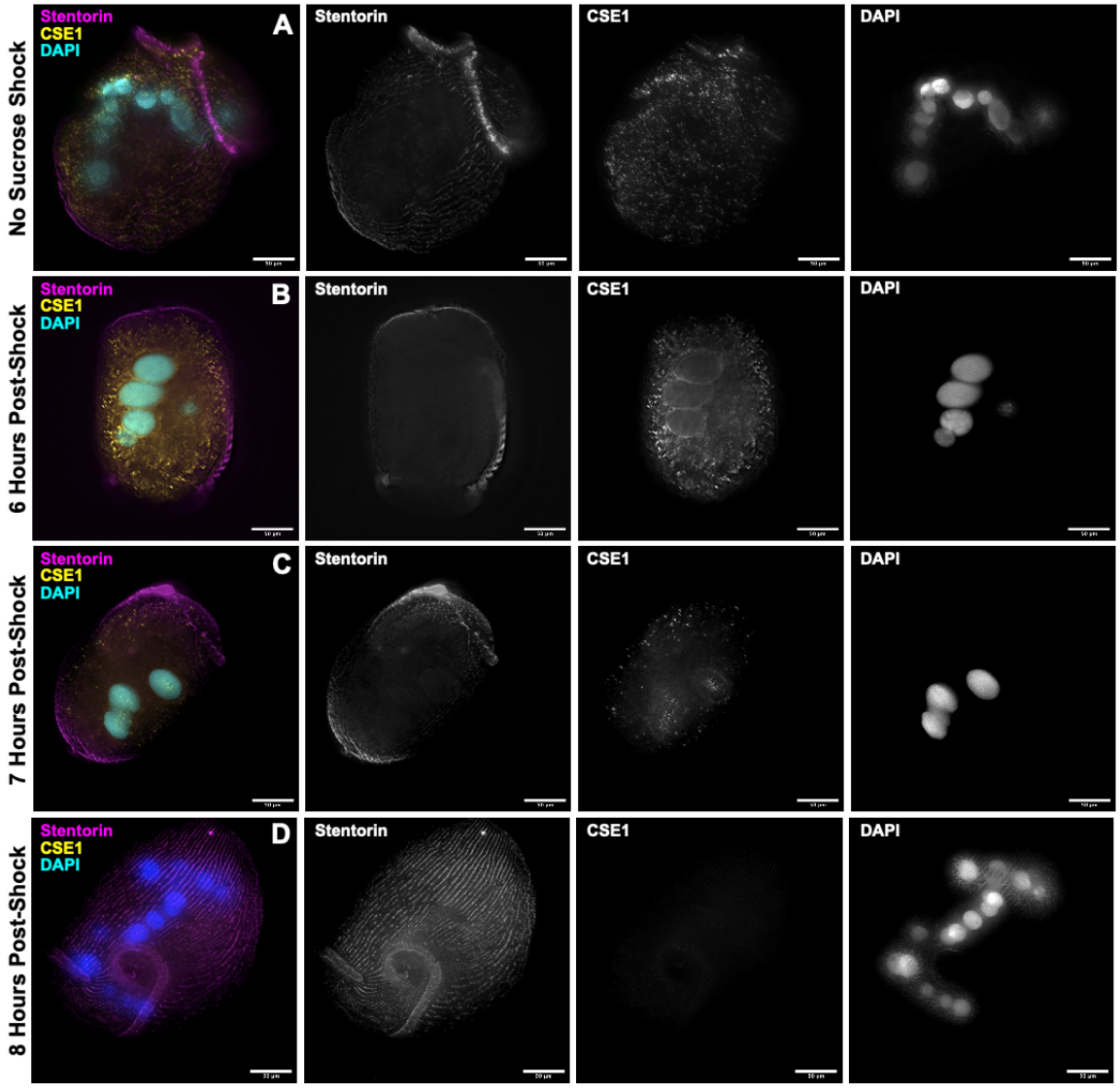

Figure 2.17: CSE1 localization CSE1 in methanol fixed *Stentor* during regeneration. All cells were imaged with a 20x air objective on a DeltaVision deconvolution microscope. (A) Stentors that have not undergone sucrose shock have cytoplasmic puncta of CSE1. (B) Six hours post sucrose shock is generally the time at which the macronucleus begins condensation. Here we observed 3 stentors with CSE1 staining around the periphery of the macronucleus. (C) At 7 hours post sucrose shock the macronucleus in this cell is condensed. At this time we observe CSE1 puncta inside of the macronucleus. (D) At 8 hours post sucrose shock, the total CSE1 signal is greatly decreased relative to pre-sucrose shock stentors. The intensity range displayed in the CSE1 image for 8 hours post sucrose shock is the same as the intensity range displayed in the non-sucrose shock CSE1 image (A).

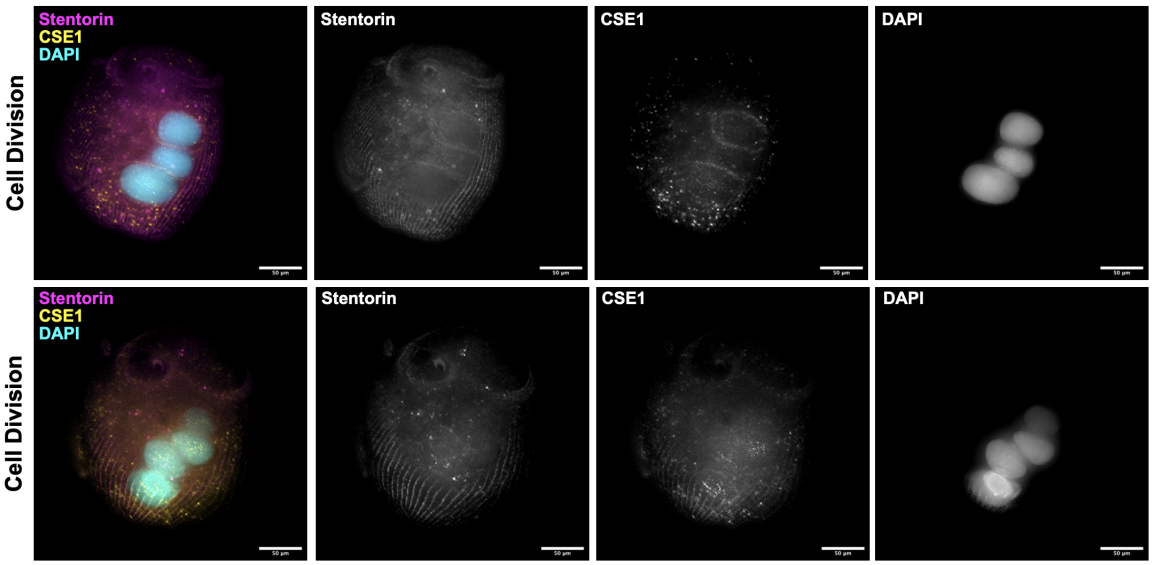

Figure 2.18: Immunofluorescence of CSE1 in dividing *Stentor* fixed with methanol. *Stentor* late in cell division are readily identifiable in culture because they have a visible membranellar band developing on the side of the cell, as well as the original membranellar band at the anterior end. Cells were imaged with a 20x air objective on a DeltaVision deconvolution microscope. In cells with condensed macronuclei we observe CSE1 around the periphery of the macronucleus, as well as punctate CSE1 staining in the interior of the macronucleus.

Table 2.1: List of RNAi constructs and primers used in this study

RNAi Name	Target Gene	Position in Coding Sequence	Forward Primer	Reverse Primer
CSE1A	CSE1 (g28374)	1247 - 2084	AACTGGAAG CAAATGGAT GC	AGCCATAGA TGAGGCATT GG
CSE1B	CSE1 (g28374)	2089 - 2841	TGCCTCATC TATGGCTCC TC	TTGAAGAGT TGGGCGTAT CG
LF4	LF4	8 - 884	CAGAATACC GTTTGATAT CAAAAAAAG GTGAAGG	CTACTTGCC TCATCAACA AAATCTTTG AAATAAGG
Mob1	Mob1	40 - 672	AAGAAGCGA ATTGAAAAA GGCCAGC	GTTACCAGA AGCTTCTCT TTCCATTCTT TCC

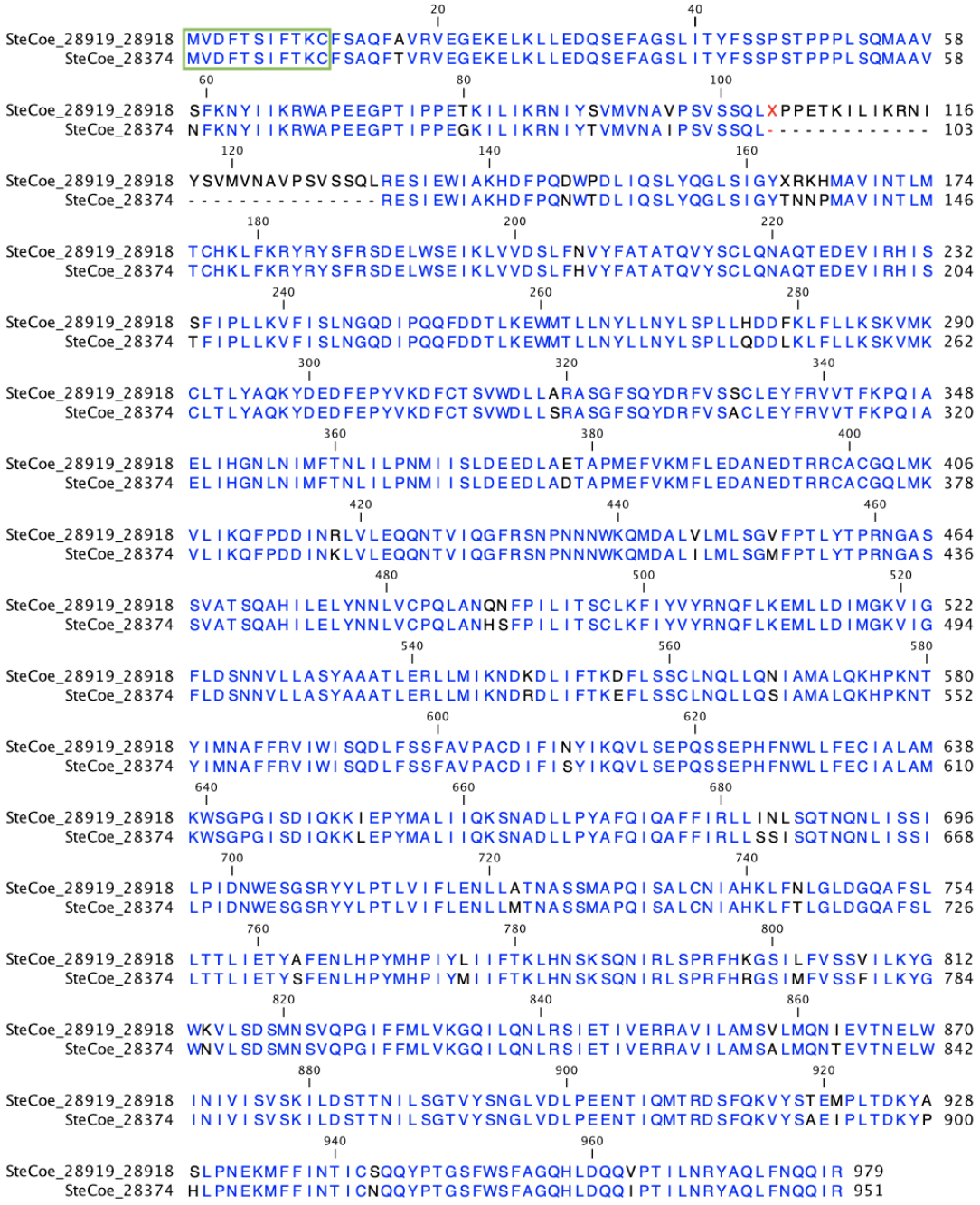

Figure 2.19: Alignment of protein sequences of *Stentor's* two CSE1 orthologs. Gene 28374 is the CSE1 gene that RNAi constructs were made against. Gene 28919+28918 is a slightly longer ortholog that is 92% identical to gene 28374. The green box shows the peptide sequence that the CSE1 antibody was raised against.

```
SteCoe_g28919+8    1 ----MVDFTSI---FTKCFSAQFAVRVEGEKELKLLEDQSEFAGSLITYFSSPSTPPPLS
SteCoe_g28374      1 ----MVDFTSI---FTKCFSAQFTVRVEGEKELKLLEDQSEFAGSLITYFSSPSTPPPLS
SacCer_CSE1        1 ----MSDLETVAKFLAESVIASTA--KTSERNLRQLETQDGFGLTLLHVIASTNLPLSTR
DroMel_CSE1        1 MEVTEANLQLLAGYLQQTLSADPNVRRPAEKLLESTELQQNYPILLLNLIDKAQMDMTTR
HomSap_CAS         1 MELSDANLQTLTEYLKKTLDPDPAIRRPAEKFLESVEGNQNYPLLLLTLLEKSQ-DNVIK
MusMus_XPO2        1 MELSDANLQTLTEYLKKTLDPDPAIRRPAEKFLESVEGNQNYPLLLLTLLEKSQ-DNVIK

SteCoe_g28919+8   54 QMAAVSFKNYIIKRW---APEEGPTIPPETKILIKRNIYSVMVNAVPSVSSQLXPPETKI
SteCoe_g28374     54 QMAAVNFKNYIIKRW---APEEGPT----------------------------IPPEGKI
SacCer_CSE1       55 LAGALFFKNFIKRKW---VDENGNH---------------------------LLPANNVE
DroMel_CSE1       61 VAGAIAFKNYIKRNWAAHLDSDGPD--------------------------RIHESDRN
HomSap_CAS        60 VCASVTFKNYIKRNW--RIVEDEPN-------------------------KICEADRV
MusMus_XPO2       60 VCASVTFKNYIKRNW--RIVEDEPN-------------------------KICEADRV

SteCoe_g28919+8  111 LIKRNIYSVMVNAVPSVSSQLRESIEWIAKHDFPQDWPDLIQSLYQGLSIGYXRKHMAVI
SteCoe_g28374     83 LIKRNIYTVMVNAIPSVSSQLRESIEWIAKHDFPQNWTDLIQSLYQGLSIGYTNNPMAVI
SacCer_CSE1       85 LIKKEIVPLMISLPNNLQVQIGEAISSIADSDFPDRWPTLLSDLASRLSND----DMVTN
DroMel_CSE1       94 TIKTLIVTLMLHSPVALQKQLSDAVSIIGKYDFPKKWPQLIDEMVERFASG----DFNVI
HomSap_CAS        91 AIKANIVHLMLSSPEQIQKQLSDAISIIGREDFPQKWPDLLTEMVNRFQSG----DFHVI
MusMus_XPO2       91 AIKANIVHLMLSSPEQIQKQLSDAISIIGREDFPQKWPDLLTEMVNRFQSG----DFHVI

SteCoe_g28919+8  171 N-TLMTCHKLFKRYRYSFRSDELWSEIKLVVDSL---FNVYFATATQVYSCLQNAQTEDE
SteCoe_g28374    143 N-TLMTCHKLFKRYRYSFRSDELWSEIKLVVDSL---FHVYFATATQVYSCLQNAQTEDE
SacCer_CSE1      141 KGVLTVAHSIFKRWRPLFRSDELFLEIKLVLDVFTAPFLNLLKTVDEQITANENNKASLN
DroMel_CSE1      150 NGVLQTAHSLFKRYRYEFKSQALWEEIKFVLDRMAKPLTDLLQATMQLTKVHENNAGALK
HomSap_CAS       147 NGVLRTAHSLFKRYRHEFKSNELWTEIKLVLDAFALPLTNLFKATIELCSTHANDASALR
MusMus_XPO2      147 NGVLRTAHSLFKRYRHEFKSNELWTEIKLVLDAFALPLTNLFKATIELCSTHANDASALR

SteCoe_g28919+8  227 VIRHISSFIPLLKVFISLNGQDIPQQFDDTLKEWMTLLNYLLNYLSPLLHDDFK------
SteCoe_g28374    199 VIRHISTFIPLLKVFISLNGQDIPQQFDDTLKEWMTLLNYLLNYLSPLLQDDLK------
SacCer_CSE1      201 IL--FDVLLVLIKLYYDFNCQDIPEFFEDNIQVGMGIFHKYLSYSNPLLEDPDETEHASV
DroMel_CSE1      210 VI--YGSLVLVNKVFFSLNSQDLPEFFEDNINTWMGAFIQQLAADVPSLRTADD-EDAGV
HomSap_CAS       207 IL--FSSLILISKLFYSLNFQDLPEFFEDNMETWMNNFHTLLTLDNKLLQTDDE-EEAGL
MusMus_XPO2      207 IL--FSSLILISKLFYSLNFQDLPEFFEDNMETWMNNFHTLLTLDNKLLQTDDE-EEAGL

SteCoe_g28919+8  281 LFLLKSKVMKCLTLYAQKYDEDFEPYVKDFCTSVWDLLARASGFSQYDRFVSSCLEYFRV
SteCoe_g28374    253 LFLLKSKVMKCLTLYAQKYDEDFEPYVKDFCTSVWDLLSRASGFSQYDRFVSACLEYFRV
SacCer_CSE1      259 LIKVKSSIQELVQLYTTRYEDVFGPMINEFIQITWNLLTSISNQPKYDILVSKSLSFLTA
DroMel_CSE1      267 LEHLRAQVCENICLYAKKYDEEFKPFMEQFVTAVWELLVKTSLHTKYDSLVSHALQFLSV
HomSap_CAS       264 LELLKSQICDNAALYAQKYDEEFQRYLPRFVTAIWNLLVTTGQEVKYDLLVSNAIQFLAS
MusMus_XPO2      264 LELLKSQICDNAALYAQKYDEEFQRYLPRFVTAIWNLLVTTGREVKYDLLVSNAIQFLAS

SteCoe_g28919+8  341 VTFKPQIAELIHGN--LNIMFTNLILPNMIISLDEEDLAETAPMEFVKMFLEDANEDTRR
SteCoe_g28374    313 VTFKPQIAELIHGN--LNIMFTNLILPNMIISLDEEDLADTAPMEFVKMFLEDANEDTRR
SacCer_CSE1      319 VTRIPKYFEIFNNESAMNNITEQIILPNVTLREEDVELFEDDPIEYIRRDLEGSDTDTRR
DroMel_CSE1      327 VADRQHYQSIFENPEILAQICDKVVIPNLDIRPSDEEIFEDSPEEYIRRDIEGSDIDTRR
HomSap_CAS       324 VCERPHYKNLFEDQNTLTSICEKVIVPNMEFRAADEEAFEDNSEEYIRRDLEGSDIDTRR
MusMus_XPO2      324 VCERPHYKNLFEDQNTLTSICEKVIVPNMEFRAADEEAFEDNSEEYIRRDLEGSDIDTRR

SteCoe_g28919+8  399 CACGQLMKVLIKQFPDDINRLVLEQQNTVIQGFRSNPNNNWKQMDALVLMLSGVFPTLYT
SteCoe_g28374    371 CACGQLMKVLIKQFPDDINKLVLEQQNTVIQGFRSNPNNNWKQMDALILMLSGMFPTLYT
SacCer_CSE1      379 RACTDFLKELKEKNEVLVTNIFLAHMKGFVDQYMSDPSKNWKFKDLYIYLFTALAINGNI
```

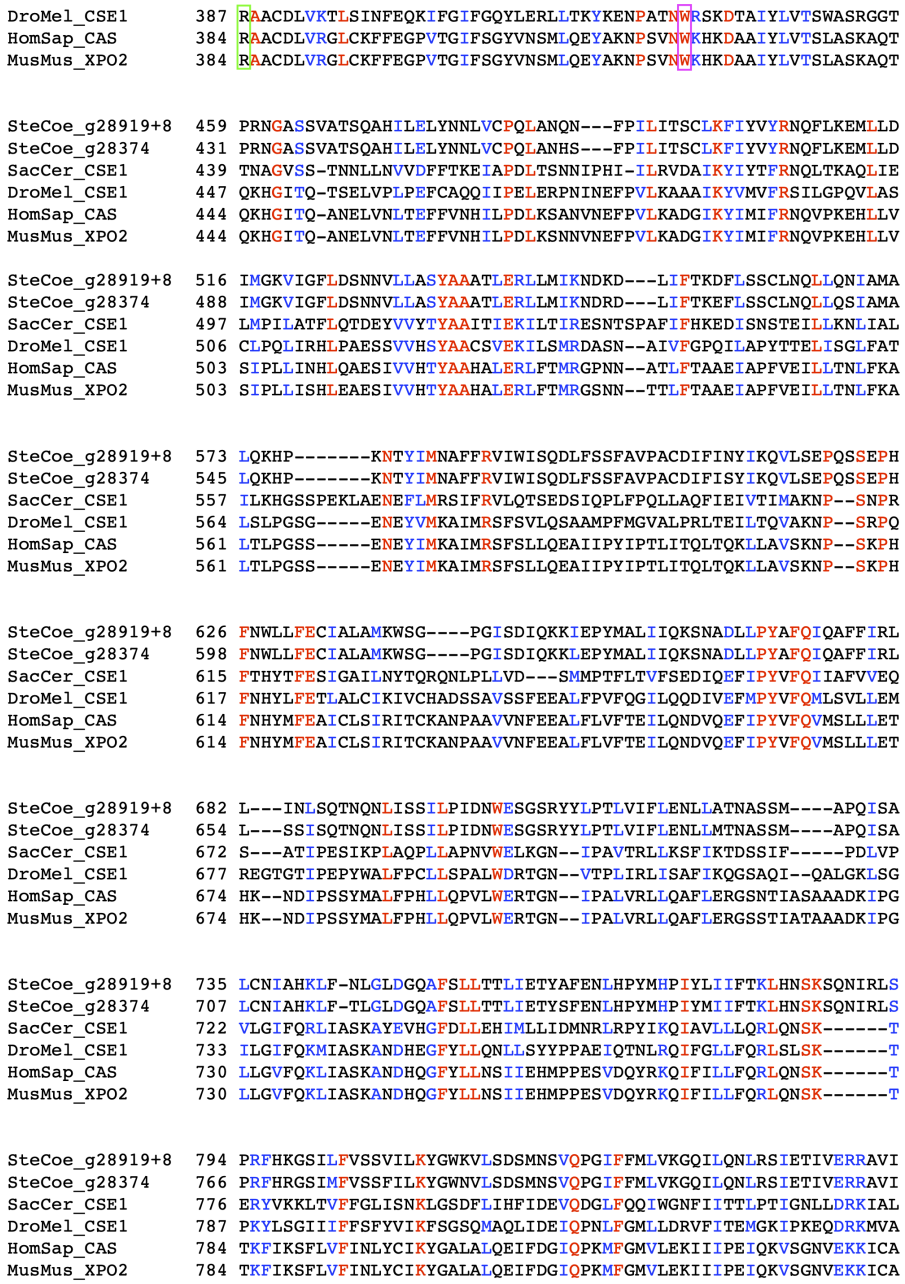
DroMel_CSE1 387 RAACDLVKTLSINFEQKIFGIFGQYLERLLTKYKENPATNWRSKDTAIYLVTSWASRGGT
HomSap_CAS 384 RAACDLVRGLCKFFEGPVTGIFSGYVNSMLQEYAKNPSVNWKHKDAAIYLVTSLASKAQT
MusMus_XPO2 384 RAACDLVRGLCKFFEGPVTGIFSGYVNSMLQEYAKNPSVNWKHKDAAIYLVTSLASKAQT
SteCoe_g28919+8 459 PRNGASSVATSQAHILELYNNLVCPQLANQN---FPILITSCLKFIYVYRNQFLKEMLLD
SteCoe_g28374 431 PRNGASSVATSQAHILELYNNLVCPQLANHS---FPILITSCLKFIYVYRNQFLKEMLLD
SacCer_CSE1 439 TNAGVSS-TNNLLNVVDFFTKEIAPDLTSNNIPHI-ILRVDAIKYIYTFRNQLTKAQLIE
DroMel_CSE1 447 QKHGITQ-TSELVPLPEFCAQQIIPELERPNINEFPVLKAAAIKYVMVFRSILGPQVLAS
HomSap_CAS 444 QKHGITQ-ANELVNLTEFFVNHILPDLKSANVNEFPVLKADGIKYIMIFRNQVPKEHLLV
MusMus_XPO2 444 QKHGITQ-ANELVNLTEFFVNHILPDLKSNNVNEFPVLKADGIKYIMIFRNQVPKEHLLV
SteCoe_g28919+8 516 IMGKVIGFLDSNNVLLASYAAATLERLLMIKNDKD---LIFTKDFLSSCLNQLLQNIAMA
SteCoe_g28374 488 IMGKVIGFLDSNNVLLASYAAATLERLLMIKNDRD---LIFTKEFLSSCLNQLLQSIAMA
SacCer_CSE1 497 LMPILATFLQTDEYVVYTYAAITIEKILTIRESNTSPAFIFHKEDISNSTEILLKNLIAL
DroMel_CSE1 506 CLPQLIRHLPAESSVVHSYAACSVEKILSMRDASN--AIVFGPQILAPYTTELISGLFAT
HomSap_CAS 503 SIPLLINHLQAESIVVHTYAAHALERLFTMRGPNN--ATLFTAAEIAPFVEILLTNLFKA
MusMus_XPO2 503 SIPLLISHLEAESIVVHTYAAHALERLFTMRGSNN--TTLFTAAEIAPFVEILLTNLFKA
SteCoe_g28919+8 573 LQKHP-------KNTYIMNAFFRVIWISQDLFSSFAVPACDIFINYIKQVLSEPQSSEPH
SteCoe_g28374 545 LQKHP-------KNTYIMNAFFRVIWISQDLFSSFAVPACDIFISYIKQVLSEPQSSEPH
SacCer_CSE1 557 ILKHGSSPEKLAENEFLMRSIFRVLQTSEDSIQPLFPQLLAQFIEIVTIMAKNP--SNPR
DroMel_CSE1 564 LSLPGSG-----ENEYVMKAIMRSFSVLQSAAMPFMGVALPRLTEILTQVAKNP--SRPQ
HomSap_CAS 561 LTLPGSS-----ENEYIMKAIMRSFSLLQEAIIPYIPTLITQLTQKLLAVSKNP--SKPH
MusMus_XPO2 561 LTLPGSS-----ENEYIMKAIMRSFSLLQEAIIPYIPTLITQLTQKLLAVSKNP--SKPH
SteCoe_g28919+8 626 FNWLLFECIALAMKWSG----PGISDIQKKIEPYMALIIQKSNADLLPYAFQIQAFFIRL
SteCoe_g28374 598 FNWLLFECIALAMKWSG----PGISDIQKKLEPYMALIIQKSNADLLPYAFQIQAFFIRL
SacCer_CSE1 615 FTHYTFESIGAILNYTQRQNLPLLVD---SMMPTFLTVFSEDIQEFIPYVFQIIAFVVEQ
DroMel_CSE1 617 FNHYLFETLALCIKIVCHADSSAVSSFEEALFPVFQGILQQDIVEFMPYVFQMLSVLLEM
HomSap_CAS 614 FNHYMFEAICLSIRITCKANPAAVVNFEEALFLVFTEILQNDVQEFIPYVFQVMSLLLET
MusMus_XPO2 614 FNHYMFEAICLSIRITCKANPAAVVNFEEALFLVFTEILQNDVQEFIPYVFQVMSLLLET
SteCoe_g28919+8 682 L---INLSQTNQNLISSILPIDNWESGSRYYLPTLVIFLENLLATNASSM----APQISA
SteCoe_g28374 654 L---SSISQTNQNLISSILPIDNWESGSRYYLPTLVIFLENLLMTNASSM----APQISA
SacCer_CSE1 672 S---ATIPESIKPLAQPLLAPNVWELKGN--IPAVTRLLKSFIKTDSSIF-----PDLVP
DroMel_CSE1 677 REGTGTIPEPYWALFPCLLSPALWDRTGN--VTPLIRLISAFIKQGSAQI--QALGKLSG
HomSap_CAS 674 HK--NDIPSSYMALFPHLLQPVLWERTGN--IPALVRLLQAFLERGSNTIASAAADKIPG
MusMus_XPO2 674 HK--NDIPSSYMALFPHLLQPVLWERTGN--IPALVRLLQAFLERGSSTIATAAADKIPG
SteCoe_g28919+8 735 LCNIAHKLF-NLGLDGQAFSLLTTLIETYAFENLHPYMHPIYLIIFTKLHNSKSQNIRLS
SteCoe_g28374 707 LCNIAHKLF-TLGLDGQAFSLLTTLIETYSFENLHPYMHPIYMIIFTKLHNSKSQNIRLS
SacCer_CSE1 722 VLGIFQRLIASKAYEVHGFDLLEHIMLLIDMNRLRPYIKQIAVLLLQRLQNSK------T
DroMel_CSE1 733 ILGIFQKMIASKANDHEGFYLLQNLLSYYPPAEIQTNLRQIFGLLFQRLSLSK------T
HomSap_CAS 730 LLGVFQKLIASKANDHQGFYLLNSIIEHMPPESVDQYRKQIFILLFQRLQNSK------T
MusMus_XPO2 730 LLGVFQKLIASKANDHQGFYLLNSIIEHMPPESVDQYRKQIFILLFQRLQNSK------T
SteCoe_g28919+8 794 PRFHKGSILFVSSVILKYGWKVLSDSMNSVQPGIFFMLVKGQILQNLRSIETIVERRAVI
SteCoe_g28374 766 PRFHRGSIMFVSSFILKYGWNVLSDSMNSVQPGIFFMLVKGQILQNLRSIETIVERRAVI
SacCer_CSE1 776 ERYVKKLTVFFGLISNKLGSDFLIHFIDEVQDGLFQQIWGNFIITTLPTIGNLLDRKIAL
DroMel_CSE1 787 PKYLSGIIIFFSFYVIKFSGSQMAQLIDEIQPNLFGMLLDRVFITEMGKIPKEQDRKMVA
HomSap_CAS 784 TKFIKSFLVFINLYCIKYGALALQEIFDGIQPKMFGMVLEKIIIPEIQKVSGNVEKKICA
MusMus_XPO2 784 TKFIKSFLVFINLYCIKYGALALQEIFDGIQPKMFGMVLEKIIIPEIQKVSGNVEKKICA

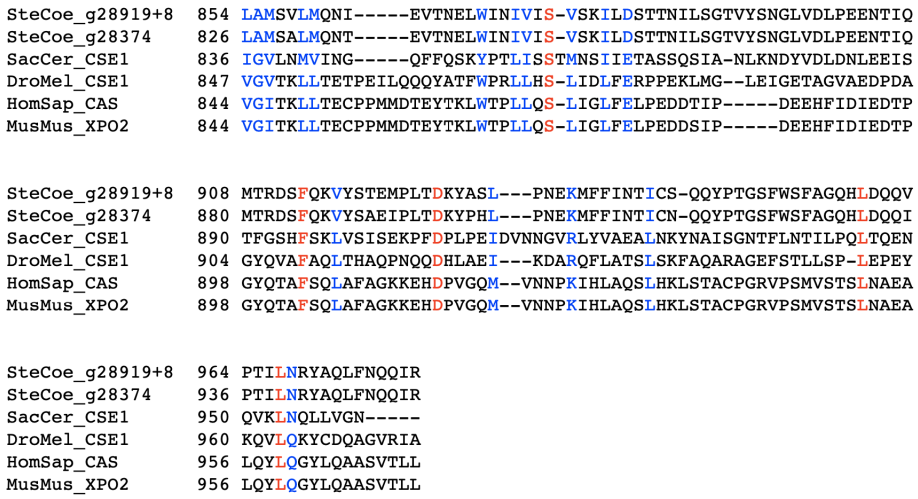

Figure 2.19: Multiple alignment of both *Stentor coeruleus* CSE1 orthologs and CSE1 homologs from *S. cerevisiae*, *D. melanogaster*, *H. sapiens*, and *M. musculus*. Mulitiple alignment performed in MEGAX using MUSCLE, displayed using Boxshade. The N-terminal half of CSE1 has multiple contact sites with importin alpha and is generally more conserved [44] [12]. In *S. cerevisiae* CSE1, the region from Asn346 to Asn379 is necessary for forming a complex with Ran-GTP and importin-alpha, and acts as a hinge between the N and C terminal halves of CSE1 (Green box) [12]. The tryptophan at position 419 in *S. cerevisiae* CSE1 is conserved in other CSE1 homologs as well as related proteins like importin betas [12]. This tryptophan is also conserved in *Stentor* CSE1 (magenta box). Asp220 in *S. cerevisiae* CSE1 has been shown to be necessary for CSE1 to form a complex with importin alpha and RanGTP – this residue is conserved (purple box) [39].

Chapter 3

Macronuclear Elongation and Nodulation

Rebecca M. McGillivary, Katherine Hammar, Wallace F. Marshall

3.1 Introduction

The macronuclear shape change cycle of *Stentor coeruleus* can be broken down into three phases: condensation, elongation, and nodulation. In chapter 2 we focused on the condensation phase, and how CSE1 is required for condensation to occur. In the course of researching *Stentor's* macronuclear shape change cycle, we have also made observations relating to the elongation and nodulation phases. These observations may be useful as starting points for more detailed investigations into these processes.

The elongation phase of the macronuclear shape change cycle has been studied previously using both microdissection experiments and electron microscopy. Noël de Terra performed most of the grafting and dissection experiments that inform our understanding of the macronuclear elongation process in *Stentor*. Her work has shown that initiation of elongation itself depends on the state of the cytoplasm. A condensed macronucleus that is transplanted to a non-regenerating cell will not elongate or nodulate normally, while a condensed macronucleus transplanted to a regenerating stentor is able to elongate [13] [18]. The macronucleus also interacts with the cortical rows - these are bundles of microtubules and cilia that run along the anterior-posterior axis of *Stentor*. The spacing of these rows vary from narrow to wide around the circumference of the cell. The region where the wide and narrow rows meet is named the locus of stripe contrast. During interphase, the macronucleus is positioned just underneath the narrowly spaced cortical rows, to the right of the cell's gullet [14]. During the macronuclear shape change cycle, the macronucleus elongates in the direction that is parallel to the overlying cortical rows [16]. If the direction of the cortical rows is altered to be perpendicular to the anterior-posterior axis of the cell, the macronucleus will elongate in the direction that the overlying rows are oriented [16]. This shows that direction of elongation of the macronucleus is regulated by a local interaction with the cortex. The molecular nature of this interaction is completely unknown. There are no known signalling molecules involved in this process, nor are there any images showing a physical link between the macronuclear envelope and the microtubule cortex.

The elongating macronucleus has also been investigated using electron microscopy. While

these studies did not show any clear connections to the cortical rows, extensive microtubule structures are built during macronuclear elongation. In *Blepharisma*, a relative of *Stentor* that also undergoes a similar macronuclear shape change, a microtubule meshwork is built around the elongating macronucleus [32]. These microtubules are close to the surface of the macronuclear envelope, and are oriented along the axis of macronuclear elongation [32]. Treating condensed *Blepharisma* macronuclei with the microtubule depolymerizing drug colchicine prevents macronuclear elongation, showing that this microtubule meshwork is necessary for elongation to occur [32]. This microtubule meshwork has also been found around elongating *Stentor* macronuclei [47] [46]. In one study, another microtubule structure was reported during macronuclear elongation. In the interior of the elongating macronucleus, double-membrane bound channels full of microtubules were imaged [46]. These microtubule channels were also oriented along the axis of elongation [46]. Because these microtubules are separated from the chromatin by the nuclear envelope, they are extranuclear microtubules. As only small sections of these microtubule channels were imaged, it is unclear if they extend all the way through the macronucleus. These microtubule channel structures were not imaged in any other electron microscopy studies of macronuclear elongation of *Stentor* or *Blepharisma* [32] [47].

3.2 Microtubules and macronuclear elongation

We imaged elongating macronuclei in *Stentor coeruleus* using transmission electron microscopy, and we were able to visualize faint microtubules around the periphery of the macronuclear envelope **(Figure 3.1 A)**. This stentor was from a strain of wild *Stentor coeruleus* that was caught from Golden Gate Park in San Francisco, CA. The stentors were sucrose shocked in a 15% sucrose solution for two minutes. The cells were incubated at room temperature for 6 hours and 20 minutes. The stentors were then fixed and imaged using the same protocol as the stentors imaged by electron micrsocopy in Chapter 2. In our images we did not observe any changes to the chromatin structure or nucleoli as was observed in Pelvat, 1982, nor did we observe the nuclear-envelope bound channels of microtubules observed in Paulin, 1975 [47] [46]. We were able to visualize some nuclear pores at the periphery of the macronucleus, as well as some faint lines protruding from the macronucleus that could be the microtubule mesh that appears around the elongating macronucleus **(Figure 3.1 A)**. In cells that were fixed 7 hours post-sucrose shock, we did not observe these microtubules **(Figure 3.1 B)**.

We also investigated these microtubule structures using immunofluoresence. This technique was not utilized in the classical literature. Using fluorescence microscopy would allow for easier sample preparation, and it would also allow us to visualize a larger region of the cell than transmission electron microscopy. Immunofluorescence still shares the disadvantage of fixation possibly disrupting these structures.

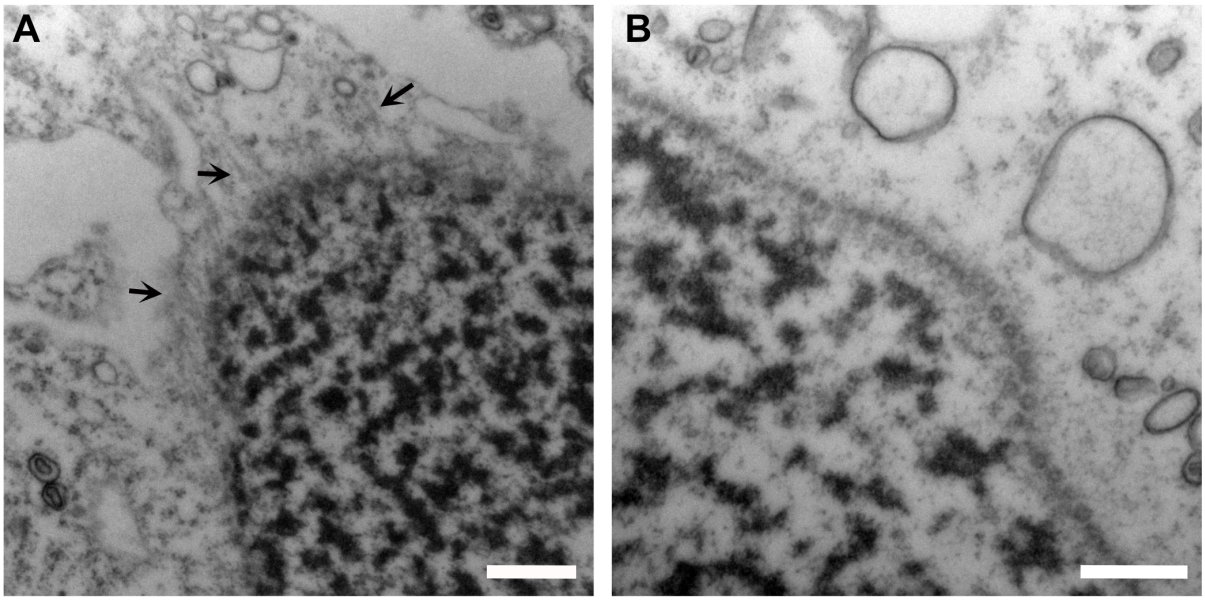

Figure 3.1: Transmission electron microscopy of elongating macronuclei. (A) A macronucleus 6 hours and 20 minutes post sucrose shock (Scale bar = 500 nm). The region with alternating dark and light patches is the chromatin. Nuclear pores, appearing like small circles, are visible surrounding the chromatin. Just outside of the nuclear pores, faint lines can be seen extending out away from the macronucleus (arrows), these are likely extranuclear microtubules. They appear similar to those found around the elongating *Blepharisma* macronucleus [32]. (B) A macronucleus 7 hours post sucrose shock (Scale bar = 500 nm). While the chromatin structure and the nuclear pores are visible, we did not observe microtubules at this timepoint.

We modified our typical methanol fixation protocol to include the addition of a 30-second rinse in microtubule stabilization buffer (80 mM PIPES pH 6.8, 1 mM MgCl2, 4 mM EGTA, 0.5% Tween 20) just before the cells were fixed in ice-cold methanol. The rest of the fixation and staining was carried out as detailed in the methods for methanol fixation in Chapter 2. We used a monoclonal anti-alpha-tubulin antibody as our primary antibody, and an anti-mouse-Alexa488 secondary antibody. The cells were imaged on a W1 spinning disk microscope equipped with a Plan Fluor 40x/1.3 oil immersion objective.

Utilizing this technique, we were able to image the outer microtubule mesh in stentors undergoing macronuclear elongation. In one case, we also observed microtubule structures inside of the macronucleus **(Figure 3.2).** The signal from these interior microtubules was much fainter than the signal coming from the microtubule cortex. Imaging these cells on a spinning disk confocal allowed us to more clearly visualize these structures without background signal from the cortical microtubules obscuring the interior microtubules. These interior microtubules appear to span the macronucleus, suggesting that the microtubules imaged in TEM studies were not small invaginations into the nuclear envelope. In this cell it does not appear that the interior microtubules are strictly aligned with the axis of elongation. While we only imaged these interior microtubules in a single cell, we noted that this cell had the most vermiform macronucleus of the cells that we imaged using this protocol. It is likely that these interior microtubules are very transient, and only present during the brief window of time in which the macronucleus is elongated but not yet nodulated. It is also likely that these structures are delicate, and are difficult to preserve during fixation. This is only the second time these interior microtubules have been imaged in 45 years [46]. While we do not have enough data about these interior microtubules to make strong biological claims about them, this observation could lead to future studies about the role of microtubules in macronuclear elongation.

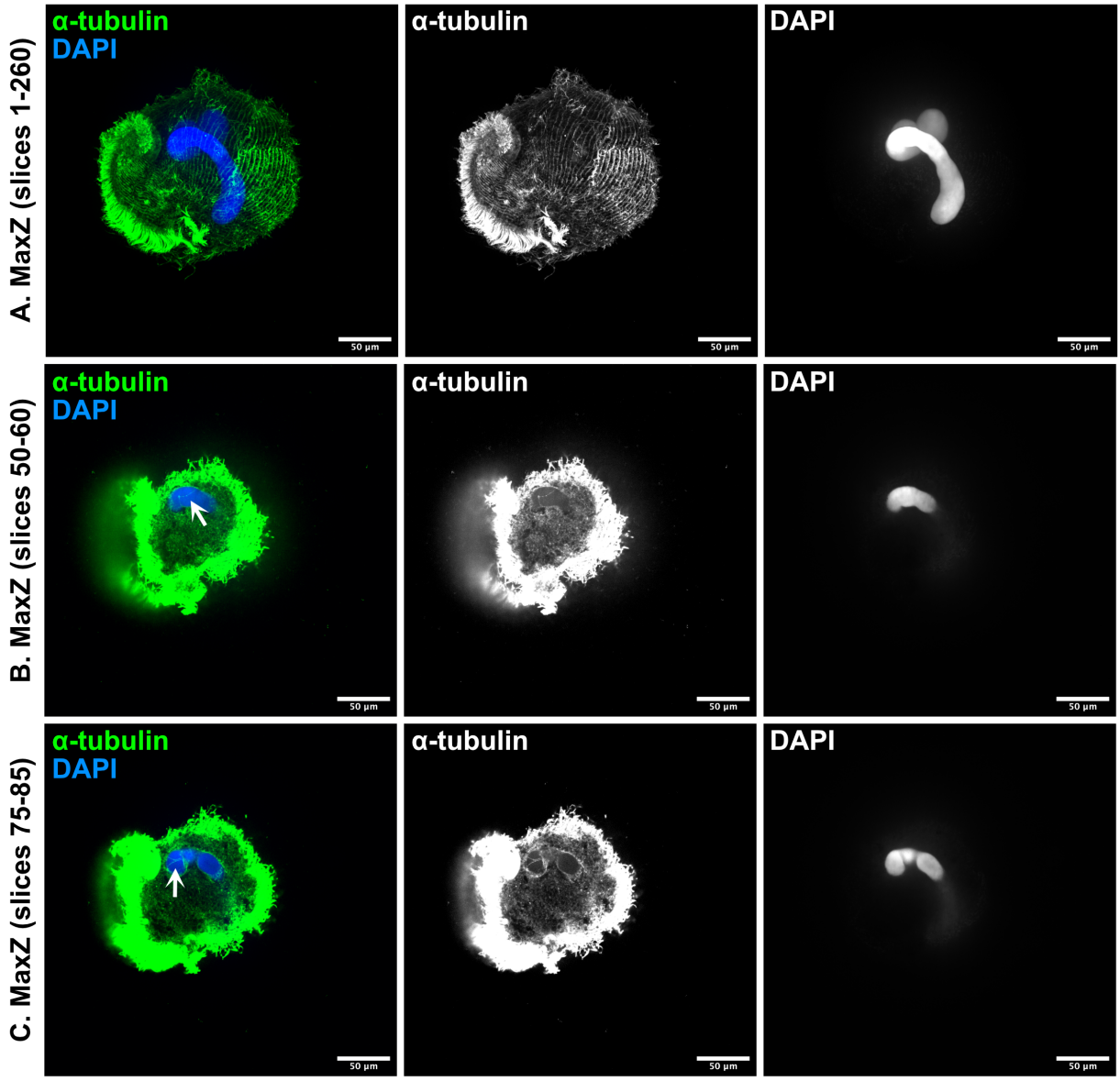

Figure 3.2: Immunofluorescence of microtubules during macronuclear elongation. (A) Max Z projection of the an entire cell that was fixed 6.5 hours after sucrose shock (Scale bars = 50 um). The macronucleus in this cell is elongated and has not undergone nodulation yet. (B) MaxZ of slices 50-60 of the cell in (A) - this region is about 3 um thick and is inside of the macronucleus. Microtubule structures can be seen spanning the macronucleus (arrow). C. MaxZ of slices 75-85 of the cell in (A) - this region is about 3 um thick and is inside of the macronucleus. A microtubule mesh surrounding the macronucleus is visible, and microtubule structures inside of the macronucleus are visible here as well (arrow).

3.3 SUN proteins and macronuclear nodulation

Of the three phases of the macronuclear shape change cycle - condensation, elongation, and nodulation - nodulation is the least studied process. Previous reports describe nodulation occurring from the ends of the macronucleus towards the center [63]. However, we observed nodulation occurring all at once in our *Stentor* **(Figure 2.3)**. In either case, it is clear that nodulation occurs rapidly. How can a single cell equally divide a roughly 400 um long organelle into 8-10 equally sized parts? Once the macronucleus is nodulated, how is this shape maintained during interphase?

We have some data that may shed light on these questions. In eukaryotic cells, the nuclear envelope is mechanically coupled to the cytoskeleton by SUN-KASH protein complexes, called the LINC complex [55]. The SUN protein is an inner nuclear membrane protein that binds to the nuclear lamina, and to the KASH protein on outer nuclear membrane. The KASH protien then binds to the cytoplasmic cytoskeleton [55]. In many model systems, the LINC complex regulates the positioning of nuclei within cells [6]. We were initially interested in whether LINC complexes are needed to position the macronucleus underneath the narrow cortical rows in *Stentor*, so we knocked down *Stentor* genes that are homologous to SUN proteins. Instead of observing a nuclear positioning defect in RNAi-treated *Stentor*, we saw a subtle nuclear shape defect. Cells fed bacteria expressing RNAi against the SUN homolog SteCoe_21380 had elongated macronuclear nodes after 7 days of feeding **(Figure 3.3)**. Control *Stentor* fed RNAi against Twi did not have elongated macronuclear nodes

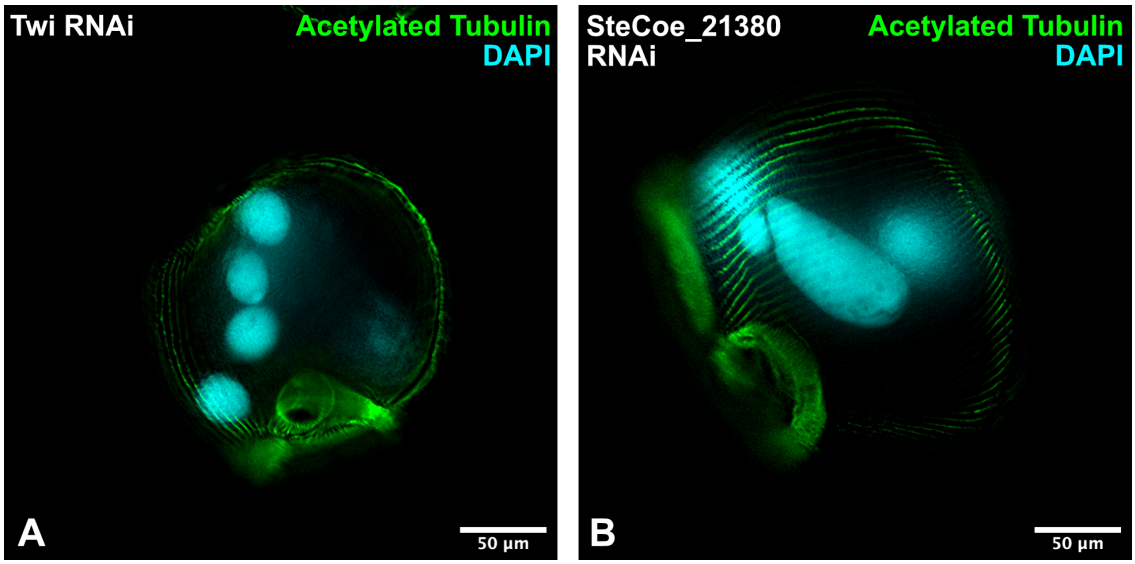

Figure 3.3: RNAi of SUN homologs in *Stentor*. (A) Control *Stentor* fed RNAi against Twi, one of *Stentor's* Argonaute genes (Scale Bar = 50 um). (B) *Stentor* fed RNAi against the SUN homolog SteCoe_21380 (Scale Bar = 50 um).

(Figure 3.3). Methanol fixation, immunofluorescence, and DAPI staining were carried out as in chapter 2. Cells were imaged on a DeltaVision deconvolution microscope with a 20x air objective. Twi RNAi downregulates *Stentor's* RNAi pathway - this control shows that the elongated nodes found in *SteCoe_21380 (RNAi)* cells are due to RNAi treatment. We also did not generally observe elongated nodes in *(LF4 RNAi)* cells **(Figure 2.8 F)**, showing that this elongated node phenotype is not due to non-specific effects from the activation of the RNAi pathway.

We manually measured the length and width of macronuclear nodes that were fully visible in both *Twi (RNAi) Stentor* and *SteCoe_21380 (RNAi) Stentor*. Due to the large size of *Stentor*, we were not able to fully image some nodes that were far away from the objective - these nodes were not measured. The average length/width ratio of *Twi (RNAi) Stentor*

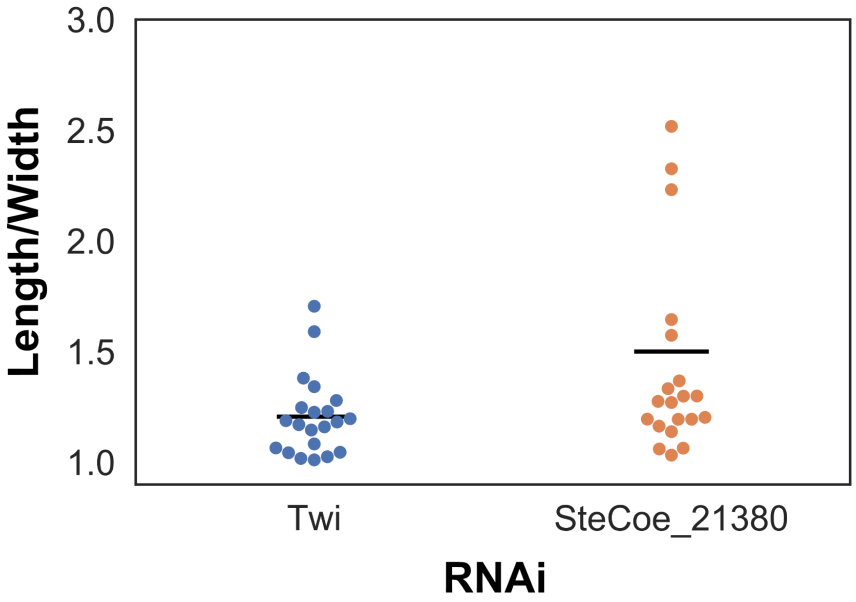

Figure 3.4: Length/width of nuclear nodes in *(SUN RNAi) Stentor*. The length and width of fully visible macronuclear nodes were measured by hand. *(Twi RNAi) Stentor* have an average length/width ratio of 1.21. *(SteCoe_21380 RNAi) Stentor* have an average length/width ratio of 1.50

was 1.21, while the average length/width ratio of *SteCoe_21380 (RNAi) Stentor* was 1.50 **(Figure 3.4)**. This increased length/width ratio in *SteCoe_21380 (RNAi) Stentor* appears to be driven by an increase in the length of the nodes, with some nodes being exceptionally long at over 90 um. The average width for both *Twi (RNAi) Stentor* and *SteCoe_21380 (RNAi) Stentor* are similar, at 25.5 um and 27.1 um, respectively. *SteCoe_21380 (RNAi) Stentor* nodes are much longer on average, at 41.5 um compared to *Twi (RNAi) Stentor's* 30.5 um. While this change in morphology is subtle, knocking down the SUN homolog SteCoe_21380 results in *Stentor* with unusually long macronuclear nodes.

3.4 Discussion

The latter half of the macronuclear shape change cycle, elongation and nodulation, are complex morphological processes that likely involve extensive interactions between the macronucleus and the cytoskeleton. Macronuclear elongation has the most clear link to the cytoskeleton, as it becomes surrounded by a microtubule mesh and elongates along the overlying cortical rows [47] [46] [16]. While it has been shown in *Blepharisma* that treatment with colchicine blocks macronuclear elongation, this experiment has not been performed on *Stentor* [32]. It is also unclear whether colchicine blocks macronuclear elongation by depolymerizing the perinuclear microtubule mesh, or by depolymerizing other cytoplasmic microtubules. The perinuclear microtubule mesh is difficult to visualize using transmission electron microscopy **(Figure 3.1)**. However, we have shown that imaging this microtubule mesh is possible using immunofluorescence **(Figure 3.2)**. Since this technique is faster to perform than transmission electron microscopy, and allows us to visualize a larger portion of the elongating macronucleus, future experiments investigating the effects of different drugs or RNAi constructs on this microtubule mesh are now feasible.

One of the most striking observations we made was the imaging of microtubules spanning the macronucleus during elongation. This has only been imaged before in a single stentor in 1975, making the cell that we imaged only the second observation of these microtubule structures [46]. In our immunofluorescence experiment we could not determine if these microtubules were surrounded by nuclear envelope as they were in the original observation [46]. In

our experiment, we could tell that these microtubules protrude deep into the macronucleus. Intranuclear channels filled with microtubules have not been described in other heterotrich ciliates. Similar structures are present in dinoflagellates - during dinomitosis, a network of membrane channels filled with microtubules act as a spindle, and the condensed chromosomes attach to the nuclear envelope, not directly to the microtubules themselves [24]. However, as *Stentor* macronuclei do not undergo mitosis, these microtubule channels cannot be directly compared to a mitotic spindle. Instead, these microtubule channels may be providing some mechanical support for this very large macronucleus during its rapid elongation - perhaps like fibers in a composite material.

Investigating this *in vivo* may be difficult because it is unclear how we could specifically disrupt these interior microtubule channels, and not the cortex and perinuclear meshwork. This would be an interesting mechanical structure to simulate *in silico*, to see if embedding fibers into a chromatin-like material allows it to withstand pulling forces so as to maintain a vermiform shape. More immunofluorescence imaging of these microtubule structures could inform these simulations by helping us learn how these fibers are oriented, and at which times during elongation they appear. If live imaging of tubulin in *Stentor* becomes feasible, we could learn about the dynamics of these structures relative to the shape change of the macronucleus. While immunofluorescence allows us to visualize the microtubule channels, their transient nature makes it difficult to know exactly when to fix the cell to image them. Live imaging would allow us to more reliably catch these unusual macronuclear structures.

Nodulation of the macronucleus is also an area that would be interesting to explore fur-

ther, as not much is known about how this part of the macronuclear shape change cycle happens. How does a single cell turn a vermiform shape into 8-10 equally sized nodes simultaneously? There are two main hypotheses for how this may happen. One hypothesis is that there may be some proteins attaching to the macronucleus that then increase the curvature of the nuclear envelope, thus squeezing the nuclear envelope into a nodular shape. Septins are an example of proteins that can sense and bind to micron-scale membrane curvature, and are a key component of the bud neck in *Saccharomyces cerevisiae* [71]. It would be interesting to see if RNAi knockdown of septin domain proteins in *Stentor* reduces the ability of the macronucleus to nodulate. It is still unclear, however, how septins or other proteins would be able to equally space themselves along the 400 um long macronucleus.

A physical model of macronuclear nodulation may be able to explain how many equally sized nodes can arise all at once. Rayleigh-Plateau instability describes how a jet of fluid can resemble a string of beads under certain conditions [22]. Random fluctuations of the surface of the liquid jet create areas of high pressure, which then pushes the liquid into areas of low pressure - this eventually creates a series of equally sized beads [22]. It is possible that a similar mechanism could nodulate the macronucleus as it is elongating. This would require the nucleoplasm in the elongating macronucleus to act like a flowing fluid - we currently have no data showing us what the dynamics of the nucleoplasm are like during elongation. While fluids with polymers added tend to have more stable node structures, it is also unclear if Rayleigh-Plateau stability is sufficient to create a nodulated macronuclear structure that lasts beyond elongation and into interphase [22]. The protein-binding model

and this physical model may not be mutually exclusive - one can imagine Rayleigh-Plateau instability creating the nodes, and a septin-like protein binding to the connections between the nodes to stabilize them. Nodulation of *Stentor's* macronucleus provides an exciting opportunity to study organelle morphogenesis from multiple perspectives.

The long-node phenotype in SUN protein knockdown *SteCoe_21380 (RNAi) Stentor* may provide a starting point to further study nodulation as well. We imaged these cells after 7 days of RNAi feeding,, and we did not sucrose shock them. We do not yet know if the long nodes are the result of incomplete nodulation after the macronuclear shape change during cell division, or if they are from a failure of *Stentor* to maintain a nodulated macronucleus over time. Imaging *SteCoe_21380 (RNAi) Stentor* during regeneration, like we did with *CSE1 (RNAi) Stentor* in chapter 2, would allow us to differentiate between these two possibilities. Since SUN proteins in other organisms are important for mechanically linking the nucleus to the cytoskeleton, it is possible that SteCoe_21380 is needed to link *Stentor's* macronucleus to either the microtubule cortex, or the microtubule mesh that appears during elongation. In transmission electron microscopy studies, it is unclear how the macronucleus is connected to either of these structures, making this an open question. While the long-node phenotype in *SteCoe_21380 (RNAi) Stentor* is subtle, combining this RNAi construct with studies on the microtubule mesh during elongation and live imaging could help us gain a greater understanding of the molecular and mechanical requirements for elongation and nodulation of the macronucleus.

The observations detailed in this chapter raise more questions than they have answered.

What is the role of microtubules during macronuclear elongation? How does the macronucleus rapidly nodulate into equally-sized nodes? How is the cytoskeleton coupled to the macronucleus? Future studies on elongation and nodulation could include an exciting combination of physical, computational, and molecular techniques.

Chapter 4

Dissertation Discussion

My work has begun to uncover the first molecular players in *Stentor coeruleus's* macronuclear shape change cycle. This nuclear shape change is remarkable for its extreme alteration in form and its rapid pace. Previous researchers, most notably Vance Tartar and Noël de Terra, investigated this process using the extremely technically difficult techniques of microdissection and grafting. Their work showed that the macronuclear shape change cycle is a regulated process that occurs during both cell division and regeneration [63]. They also showed that these regulatory signals were transmitted through both the cytoplasm and the microtubule cortex [63] [18] [16]. Their work did not show what the identity of these signals were, or how they might influence the macronuclear shape change cycle. Thanks to the sequencing of *Stentor's* genome, the development of RNAi, and RNA sequencing of genes expressed during regeneration, I was able to investigate which genes are involved in the macronuclear shape change cycle [52] [53] [54].

4.1 CSE1's role in macronuclear condensation

In chapter 2, I identified CSE1 as a protein that is necessary for macronuclear condensation to occur. This work led to a model for how CSE1 helps the macronucleus condense. Nuclear import of proteins driven by CSE1 may increase the amount of proteins present in the macronucleus, thus increasing its volume. As the volume increases rapidly, the moniliform macronucleus begins to change its shape into a sphere so that it can accommodate this increased nuclear volume with a minimal change in surface area. It has been shown in other organisms that increasing nuclear import can increase the volume of nuclei [40] [37] [8]. Here I have shown that, in *Stentor*, altering nuclear transport can alter both the volume and the shape of the macronucleus.

Currently, most studies on nuclear shape focus on the nuclear lamina and chromatin, as these parts are known to greatly affect the mechanical properties of the nucleus in various cell types [57] [43]. It would be interesting to investigate if nuclear transport also contributes to shaping nuclei in metazoan and fungal cells. Would disrupting the balance between nuclear volume and surface area re-shape a spherical nucleus? Or is there something unique about the architecture of *Stentor's* macronucleus that leaves it especially sensitive to changes in nuclear volume? It is possible that the unusual moniliform shape of *Stentor's* macronucleus makes any shape change especially obvious. Another possibility is that the size and composition of the macronucleus is so different from metazoan nuclei that it behaves in fundamentally different ways from most metazoan nuclei. *Stentor's* macronucleus is approximately 150

times larger by volume than a U2OS cell nucleus [35]. *Stentor* also does not have any homologs to lamins - it is unclear if *Stentor* has any proteins that fulfill a similar role. In transmission electron microscopy studies, there have been no observations of peripheral heterochromatin like one would find in most metazoan cells [47] **(Figure 2.1 C).** *Stentor's* macronucleus is two orders of magnitude larger than typical metazoan nuclei, and it does not possess a lamina or chromatin structure that is similar to metazoan nuclei. Future studies on the mechanobiology of *Stentor's* macronucleus, the composition of its macronuclear envelope, and the structure of its chromatin would help us gain a better understanding of how this giant nucleus can be greatly re-shaped by alterations in nuclear transport.

4.2 Future directions for the study of elongation and nodulation

In chapter 3, I report observations that relate to the elongation and nodulation phases of the macronuclear shape change cycle. These observations can provide footholds for future investigations of macronuclear elongation and nodulation. These observations on their own do not provide enough information to build models for how elongation and nodulation are regulated. However, taken together with the classical literature, it appears that elongation and nodulation require a large amount of force transduction, likely through the microtubule cytoskeleton [46] [47].

In chapter 2, I found that the volume of the macronucleus decreases during elongation, and that CSE1 levels also drop. This suggests that the macronucleus's reduction in volume makes it possible to remodel it into a non-spherical shape. Stretching the macronucleus into a long vermiform shape that can reach across the cell requires force transduction - the perinuclear microtubule meshwork and the microtubule channels that appear during this time are likely candidates for this force-transduction role. Future work will be needed to determine whether these structures are necessary for elongation to occur, and if so, to determine how this force is generated and transmitted.

Given the prominence of microtubules during macronuclear elongation, it was interesting that RNAi knockdown of a SUN protein homolog produced a subtle defect in nodulation of the macronucleus. SUN proteins are part of the LINC complex, which connects the nuclear envelope to the cytoskeleton. Future work is needed to determine if the LINC complex in *Stentor* is needed to transmit force from the cytoskeleton to the macronucleus during elongation, nodulation, and/or maintenance of the macronuclear nodes during interphase.

The macronuclear shape change cycle in *Stentor coeruleus* is a fascinating model for the study of nuclear shape. Here I have identified the first gene needed for macronuclear condensation to occur, CSE1. I have also reported observations that can lead to future studies on the latter half of the macronuclear shape change cycle: elongation and nodulation. There is much more to be discovered on how *Stentor* is able to dramatically re-shape its nucleus. It is clear that there is a rich variety of molecular and physical mechanisms regulating the different phases of this extreme nuclear shape change.

References

[1] S F Altschul et al. "Basic local alignment search tool". en. In: *J. Mol. Biol.* 215.3 (Oct. 1990), pp. 403–410.

[2] Cori A Anderson et al. "Nuclear repulsion enables division autonomy in a single cytoplasm". en. In: *Curr. Biol.* 23.20 (Oct. 2013), pp. 1999–2010.

[3] Hannah E Arbach et al. "Extreme nuclear branching in healthy epidermal cells of the Xenopus tail fin". en. In: *J. Cell Sci.* 131.18 (Sept. 2018).

[4] C Aslanidis and P J de Jong. "Ligation-independent cloning of PCR products (LIC-PCR)". en. In: *Nucleic Acids Res.* 18.20 (Oct. 1990), pp. 6069–6074.

[5] Matthias Blum et al. "The InterPro protein families and domains database: 20 years on". en. In: *Nucleic Acids Res.* 49.D1 (Jan. 2021), pp. D344–D354.

[6] Courtney R Bone and Daniel A Starr. "Nuclear migration events throughout development". en. In: *J. Cell Sci.* 129.10 (May 2016), pp. 1951–1961.

[7] Courtney R Bone et al. “Nuclei migrate through constricted spaces using microtubule motors and actin networks in C. elegans hypodermal cells”. en. In: *Development* 143.22 (Nov. 2016), pp. 4193–4202.

[8] Vincent Boudreau et al. “Nucleo-cytoplasmic trafficking regulates nuclear surface area during nuclear organogenesis”. en. May 2018.

[9] J C Bruusgaard et al. “Number and spatial distribution of nuclei in the muscle fibres of normal mice studied in vivo”. en. In: *J. Physiol.* 551.Pt 2 (Sept. 2003), pp. 467–478.

[10] Leonardo Olivieri Carvalho et al. “The Neutrophil Nucleus and Its Role in Neutrophilic Function”. en. In: *J. Cell. Biochem.* 116.9 (Sept. 2015), pp. 1831–1836.

[11] Yee-Hung M Chan and Wallace F Marshall. “Scaling properties of cell and organelle size”. en. In: *Organogenesis* 6.2 (Apr. 2010), pp. 88–96.

[12] Atlanta Cook et al. “The structure of the nuclear export receptor Cse1 in its cytosolic state reveals a closed conformation incompatible with cargo binding”. en. In: *Mol. Cell* 18.3 (Apr. 2005), pp. 355–367.

[13] N De Terra. *A Study of Nucleo-cytoplasmic Interactions During Cell Division in Stentor coeruleus*. 1960.

[14] Noel De Terra. “Cortical Control of Macronuclear Positioning in the Ciliate Stentor”. In: *J. Exp. Zool.* 216 (1981), pp. 367–376.

[15] Noel De Terra. "Cortical control of macronuclear positioning in the ciliate Stentor". In: *J. Exp. Zool.* 216.3 (1981), pp. 367–376.

[16] Noel De Terra. "Cortical Control over the Direction of Macronuclear Elongation in the Heterotrich Ciliate Stentor coeruleus". In: *J. Protozool.* 30.2 (1983), pp. 215–217.

[17] Noel De Terra. "Macronuclear DNA Synthesis in Stentor: Regulation by a Cytoplasmic Initiator". In: *Proc. N. A. S.* 57 (1966), pp. 607–614.

[18] Noel De Terra. "Nucleocytoplasmic Interactions during the Differentiation of Oral Structures in Stentor coeruleus". In: *Developmental Biology* 10 (1964), pp. 269–288.

[19] Samantha E R Dundon et al. "Clustered nuclei maintain autonomy and nucleocytoplasmic ratio control in a syncytium". en. In: *Mol. Biol. Cell* 27.13 (July 2016), pp. 2000–2007.

[20] Arthur D Edelstein et al. "Advanced methods of microscope control using μManager software". en. In: *J Biol Methods* 1.2 (2014).

[21] Eric S Folker and Mary K Baylies. "Nuclear positioning in muscle development and disease". In: *Front. Physiol.* 4 (Dec. 2013), p. 363.

[22] François Gallaire and P-T Brun. "Fluid dynamic instabilities: theory and application to pattern forming in complex media". en. In: *Philos. Trans. A Math. Phys. Eng. Sci.* 375.2093 (May 2017).

[23] Feng Gao and Laura A Katz. "Phylogenomic analyses support the bifurcation of ciliates into two major clades that differ in properties of nuclear division". en. In: *Mol. Phylogenet. Evol.* 70 (Jan. 2014), pp. 240–243.

[24] Gregory S Gavelis et al. "Dinoflagellate nucleus contains an extensive endomembrane network, the nuclear net". en. In: *Sci. Rep.* 9.1 (Jan. 2019), p. 839.

[25] Robert D Goldman et al. "Accumulation of mutant lamin A causes progressive changes in nuclear architecture in Hutchinson-Gilford progeria syndrome". en. In: *Proc. Natl. Acad. Sci. U. S. A.* 101.24 (June 2004), pp. 8963–8968.

[26] Sandrine Grava et al. "Clustering of nuclei in multinucleated hyphae is prevented by dynein-driven bidirectional nuclear movements and microtubule growth control in Ashbya gossypii". en. In: *Eukaryot. Cell* 10.7 (July 2011), pp. 902–915.

[27] Stéphane Guindon and Olivier Gascuel. "A simple, fast, and accurate algorithm to estimate large phylogenies by maximum likelihood". en. In: *Syst. Biol.* 52.5 (Oct. 2003), pp. 696–704.

[28] Charles R Harris et al. "Array programming with NumPy". en. In: *Nature* 585.7825 (Sept. 2020), pp. 357–362.

[29] Jose I de las Heras and Eric C Schirmer. "The Nuclear Envelope and Cancer: A Diagnostic Perspective and Historical Overview". In: *Cancer Biology and the Nuclear Envelope: Recent Advances May Elucidate Past Paradoxes*. Ed. by Eric C Schirmer and Jose I de las Heras. New York, NY: Springer New York, 2014, pp. 5–26.

[30] J K Hood and P A Silver. "Cse1p is required for export of Srp1p/importin-alpha from the nucleus in Saccharomyces cerevisiae". In: *J. Biol. Chem.* 273.52 (Dec. 1998), pp. 35142–35146.

[31] John D Hunter. "Matplotlib: A 2D Graphics Environment". In: *Computing in Science Engineering* 9.3 (May 2007), pp. 90–95.

[32] R A Jenkins. "The Role of Microtubules in Macronuclear Division of Blepharisma". In: *J. Protozool.* 24.2 (1977), pp. 264–275.

[33] D T Jones, W R Taylor, and J M Thornton. "The rapid generation of mutation data matrices from protein sequences". en. In: *Comput. Appl. Biosci.* 8.3 (June 1992), pp. 275–282.

[34] Thomas Kluyver et al. "Jupyter Notebooks – a publishing format for reproducible computational workflows". In: *Positioning and Power in Academic Publishing: Players, Agents and Agendas*. IOS Press, 2016, pp. 87–90.

[35] Britta Koch et al. "Confinement and deformation of single cells and their nuclei inside size-adapted microtubes". en. In: *Adv. Healthc. Mater.* 3.11 (Nov. 2014), pp. 1753–1758.

[36] Sudhir Kumar et al. "MEGA X: Molecular Evolutionary Genetics Analysis across Computing Platforms". en. In: *Mol. Biol. Evol.* 35.6 (June 2018), pp. 1547–1549.

[37] Kazunori Kume et al. "A systematic genomic screen implicates nucleocytoplasmic transport and membrane growth in nuclear size control". en. In: *PLoS Genet.* 13.5 (May 2017), e1006767.

[38] U Kutay et al. "Export of importin alpha from the nucleus is mediated by a specific nuclear transport factor". In: *Cell* 90.6 (Sept. 1997), pp. 1061–1071.

[39] Allison Lange et al. "Dissecting the roles of Cse1 and Nup2 in classical NLS-cargo release in vivo". en. In: *Traffic* 21.10 (Oct. 2020), pp. 622–635.

[40] Daniel L Levy and Rebecca Heald. "Nuclear size is regulated by importin α and Ntf2 in Xenopus". en. In: *Cell* 143.2 (Oct. 2010), pp. 288–298.

[41] Athena Lin et al. "Methods for the Study of Regeneration in Stentor". en. In: *J. Vis. Exp.* 136 (June 2018).

[42] "Phylum CILIOPHORA – Conjugating, Ciliated Protists with Nuclear Dualism". In: *The Ciliated Protozoa: Characterization, Classification, and Guide to the Literature.* Ed. by Denis H Lynn. Dordrecht: Springer Netherlands, 2008, pp. 89–120.

[43] Harriet R Manley, Maria Cristina Keightley, and Graham J Lieschke. "The Neutrophil Nucleus: An Important Influence on Neutrophil Migration and Function". en. In: *Front. Immunol.* 9 (Dec. 2018), p. 2867.

[44] Yoshiyuki Matsuura and Murray Stewart. "Structural basis for the assembly of a nuclear export complex". In: *Nature* 432.7019 (Dec. 2004), pp. 872–877.

[45] L P Ovchinnikova, G V Selivanova, and E M Cheissin. "Photometric study of the DNA content in the nuclei of Spirostomum ambiguum (Ciliata, Heterotricha)". In: *Acta Protozool.* 3.7 (1965), pp. 69–78.

[46] J J Paulin and A S Brooks. "Macronuclear differentiation during oral regeneration in Stentor coeruleus". In: *J. Cell Sci.* 19.3 (1975), pp. 531–541.

[47] Bernard Pelvat and Rosemarie Emery. "La Régénération de L'appareil Oral chez Stentor Coeruleus: II - Modifications de L'ultrastructure du Macronoyau". In: *Protistologica* 18.3 (1982), pp. 371–387.

[48] Jeff Reback et al. *pandas-dev/pandas: Pandas 1.0.3*. Mar. 2020.

[49] William Roman and Edgar R Gomes. "Nuclear positioning in skeletal muscle". en. In: *Semin. Cell Dev. Biol.* 82 (Oct. 2018), pp. 51–56.

[50] Paola Scaffidi and Tom Misteli. "Lamin A-dependent nuclear defects in human aging". en. In: *Science* 312.5776 (May 2006), pp. 1059–1063.

[51] Johannes Schindelin et al. "Fiji: an open-source platform for biological-image analysis". en. In: *Nat. Methods* 9.7 (June 2012), pp. 676–682.

[52] Mark M Slabodnick et al. "The kinase regulator mob1 acts as a patterning protein for stentor morphogenesis". en. In: *PLoS Biol.* 12.5 (May 2014), e1001861.

[53] Mark M Slabodnick et al. "The Macronuclear Genome of Stentor coeruleus Reveals Tiny Introns in a Giant Cell". In: *Curr. Biol.* 27.4 (2017), pp. 569–575.

[54] Pranidhi Sood et al. “Modular, Cascade-like Transcriptional Program of Regeneration in Stentor”. en. June 2021.

[55] Daniel A Starr and Heidi N Fridolfsson. “Interactions between nuclei and the cytoskeleton are mediated by SUN-KASH nuclear-envelope bridges”. en. In: *Annu. Rev. Cell Dev. Biol.* 26 (2010), pp. 421–444.

[56] Glen Stecher, Koichiro Tamura, and Sudhir Kumar. “Molecular Evolutionary Genetics Analysis (MEGA) for macOS”. en. In: *Mol. Biol. Evol.* 37.4 (Apr. 2020), pp. 1237–1239.

[57] Andrew D Stephens, Edward J Banigan, and John F Marko. “Chromatin’s physical properties shape the nucleus and its functions”. en. In: *Curr. Opin. Cell Biol.* 58 (June 2019), pp. 76–84.

[58] Andrew D Stephens et al. “Chromatin histone modifications and rigidity affect nuclear morphology independent of lamins”. en. In: *Mol. Biol. Cell* 29.2 (Jan. 2018), pp. 220–233.

[59] Andrew C Tamashunas et al. “High-throughput gene screen reveals modulators of nuclear shape”. en. In: *Mol. Biol. Cell* 31.13 (June 2020), pp. 1392–1402.

[60] V Tartar. “Equivalence of macronuclear nodes”. en. In: *J. Exp. Zool.* 135.2 (July 1957), pp. 387–401.

[61] V Tartar. “Reactions of Stentor coeruleus to Certain Substances Added to the Medium”. In: *Experimental Cell Research* 13 (1957), pp. 317–332.

[62] Vance Tartar. "Extreme Alteration of the Nucleocytoplasmic Ratio in *Stentor coeruleus* *". In: *J. Protozool.* 10.4 (Nov. 1963), pp. 445–461.

[63] Vance Tartar. *The Biology of Stentor*. New York: Pergamon Press, 1961, p. 434.

[64] Hildegard Tekotte et al. "Dcas Is Required for importin-3 Nuclear Export and Mechano-Sensory Organ Cell Fate Specification in Drosophila". In: *Dev. Biol.* 244 (2002), pp. 396–406.

[65] Alison D Walters et al. "Nuclear envelope expansion in budding yeast is independent of cell growth and does not determine nuclear volume". en. In: *Mol. Biol. Cell* 30.1 (Jan. 2019), pp. 131–145.

[66] Michael Waskom. "seaborn: statistical data visualization". In: *J. Open Source Softw.* 6.60 (Apr. 2021), p. 3021.

[67] P B Weisz. "The role of specific macronuclear nodes in the differentiation and the maintenance of the oral area in Stentor". en. In: *J. Exp. Zool.* 111.1 (June 1949), pp. 141–155.

[68] Paul B Weisz. "A cytochemical and cytological study of differentiation in normal and reorganizational stages of Stentor coeruleus". In: *J. Morphol.* 84.2 (Mar. 1949), pp. 335–363.

[69] Paul B Weisz. "Experiments on the initiation of division in Stentor coeruleus". en. In: *J. Exp. Zool.* 131.1 (Feb. 1956), pp. 137–162.

[70] D Wloga et al. “Septins stabilize mitochondria in Tetrahymena thermophila”. en. In: *Eukaryot. Cell* 7.8 (Aug. 2008), pp. 1373–1386.

[71] Benjamin L Woods and Amy S Gladfelter. “The state of the septin cytoskeleton from assembly to function”. en. In: *Curr. Opin. Cell Biol.* 68 (Feb. 2021), pp. 105–112.

[72] Jessica A Zinskie et al. “A mechanical microcompressor for high resolution imaging of motile specimens”. en. In: *Exp. Cell Res.* 337.2 (Oct. 2015), pp. 249–256.

Publishing Agreement

It is the policy of the University to encourage open access and broad distribution of all theses, dissertations, and manuscripts. The Graduate Division will facilitate the distribution of UCSF theses, dissertations, and manuscripts to the UCSF Library for open access and distribution. UCSF will make such theses, dissertations, and manuscripts accessible to the public and will take reasonable steps to preserve these works in perpetuity.

I hereby grant the non-exclusive, perpetual right to The Regents of the University of California to reproduce, publicly display, distribute, preserve, and publish copies of my thesis, dissertation, or manuscript in any form or media, now existing or later derived, including access online for teaching, research, and public service purposes.

DocuSigned by:
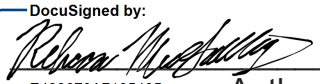
E433670A7135485...
Author Signature

10/21/2021
Date